Title
HLA-independent T cell receptors for targeting tumors with low antigen density.

Journal
Nature Medicine, 28(2)

Authors
Mansilla-Soto, Jorge
Eyquem, Justin
Haubner, Sascha
et al.

Publication Date
2022-02-01

DOI
10.1038/s41591-021-01621-1

Peer reviewed

HHS Public Access

Author manuscript

Nat Med. Author manuscript; available in PMC 2023 February 01.

Published in final edited form as:

Nat Med. 2022 February ; 28(2): 345–352. doi:10.1038/s41591-021-01621-1.

HLA-independent T cell receptors for targeting tumors with low antigen density

Jorge Mansilla-Soto[1,2,7,*], **Justin Eyquem**[1,2,7,8], **Sascha Haubner**[1,2], **Mohamad Hamieh**[1,2], **Judith Feucht**[1,2,9], **Noémie Paillon**[3], **Andrés Ernesto Zucchetti**[3], **Zhuoning Li**[4], **Maria Sjöstrand**[1,2], **Pieter L. Lindenbergh**[1,2], **Michelle Saetersmoen**[1,2,10], **Anton Dobrin**[1,2], **Mathieu Maurin**[3], **Archana Iyer**[1,2], **Andreina Garcia Angus**[1,2], **Matthew M. Miele**[4], **Zeguo Zhao**[1,2], **Theodoros Giavridis**[1,2,11], **Sjoukje J.C. van der Stegen**[1,2], **Fella Tamzalit**[2], **Isabelle Rivière**[1,5,6], **Morgan Huse**[2], **Ronald C. Hendrickson**[4,6], **Claire Hivroz**[3], **Michel Sadelain**[1,2,*]

[1.]Center for Cell Engineering, Memorial Sloan Kettering Cancer Center, New York, NY, USA

[2.]Immunology Program, Sloan Kettering Institute, New York, NY, USA

[3.]Institute Curie, Université PSL, U932 INSERM, Integrative Analysis of T cell Activation Team, Paris, France

[4.]Microchemistry and Proteomics Core Laboratory, Sloan Kettering Institute, New York, NY, USA

[5.]Cell Therapy and Cell Engineering Facility, Memorial Sloan Kettering Cancer Center, New York, NY, USA

[6.]Molecular Pharmacology Program, Memorial Sloan Kettering Cancer Center, New York, NY, USA

[7.]These authors contributed equally: Jorge Mansilla-Soto and Justin Eyquem.

[8.]Present Address: Department of Medicine, Division of Hemato-Oncology, University of California San Francisco, San Francisco, CA, USA.

[9.]Present address: Department of Cancer Immunology, Institute for Cancer Research, Oslo University Hospital, Oslo, Norway

[10.]Present address: Cluster of Excellence iFIT, University Children's Hospital Tübingen, Germany.

[11.]Present address: Mnemo Therapeutics, New York, NY, USA

Abstract

[*]Correspondence: m-sadelain@ski.mskcc.org; mansillj@mskcc.org.

Author contributions J.M-S and J.E. designed the study, performed experiments, analysed and interpreted data, and wrote the manuscript. S.H. designed and performed experiments, and analysed data. M.H., J.F., N.P., A.E.Z., Z.L, M.S., P.L.L., M. Saetersmoen, A.D., and M.M. performed experiments and analysed data. A.I. performed statistical analysis. A.G.A., M.M.M., Z.Z., T.G., S.J.C.v.d.S., and F.T., performed experiments. M.Huse designed experiments. I. R., R.C.H. and C.H. designed experiments and interpreted data. M.S. designed the study, analysed and interpreted data, and wrote the manuscript.

Competing interests Memorial Sloan Kettering has submitted a patent application based in part on results presented in this manuscript (WO2019157454A1, J.M.-S., J.E. and M.S. are listed among the inventors). R.C.H. reports stock ownership in Merck. M.S. reports research funding from Juno Therapeutics, Fate Therapeutics, Takeda Pharmaceuticals and Atara Biotherapeutics, unrelated to the present research. M.S., I.R., and J.E. are scientific co-founders of Mnemo Therapeutics. M.S. serves on the scientific advisory board of St Jude Children Research Hospital. All other authors declare no competing interests.

Chimeric antigen receptors (CARs) are receptors for antigen that direct potent immune responses. Tumour escape associated with low target antigen expression is emerging as one potential limitation of their efficacy. Here we edit the *TRAC* locus in human peripheral blood T cells to engage cell-surface targets through their TCR/CD3 complex reconfigured to utilize the same immunoglobulin heavy and light chains as a matched CAR. We demonstrate that these HLA-independent TCRs (HIT receptors) consistently afford high antigen sensitivity and mediate tumour recognition beyond what CD28-based CARs, the most sensitive design to date, can provide. We demonstrate that the functional persistence of HIT T cells can be augmented by constitutive co-expression of CD80 and 4-1BBL. Finally, we validate the increased antigen sensitivity afforded by HIT receptors in xenograft mouse models of B cell leukaemia and acute myeloid leukaemia, targeting CD19 and CD70, respectively. Overall, HIT receptors are well suited for targeting cell surface antigens of low abundance.

Introduction

CARs are synthetic receptors that redirect the specificity and augment the therapeutic potency of T lymphocytes[1]. CARs engage antigen independently of HLA[2,3] but only enable sustained T cell proliferation if they are endowed with both activating and costimulatory functions[4,5]. CD19-specific CARs that include either CD28 or 4-1BB costimulatory signaling domains have demonstrated remarkable efficacy in patients with relapsed and refractory acute lymphoblastic leukemia (ALL) or non-Hodgkin lymphoma[6-8]. CARs targeting CD22 or BCMA have also elicited major responses in patients with refractory ALL and multiple myeloma (MM), respectively[9-11]. While remission rates have been noticeably elevated in numerous clinical trials, relapses are common[10-16]. One of the several underlying relapse mechanisms is antigen escape[9,10,17-20], which refers to a relapsing tumor that is either negative for the targeted antigen or expresses the latter at a low level. Whereas CAR T cells cannot directly engage tumors with complete antigen loss, the failure to eliminate antigen-low tumors raises questions about the sensitivity of CARs and the minimum antigen density that is required for effective tumor eradication.

Recent studies have determined that all CARs are not equal in terms of their antigen sensitivity. Comparing CARs specific for different antigens, we and others have observed that CD28-based CARs are more sensitive than those incorporating 4-1BB signaling domains in cytotoxicity assays[21-23]. In *in vivo* models of antigen escape, a CD28-based CAR was more adept to control the relapse of CD19-low ALL than the corresponding 4-1BB CAR[21,22]. These archetypal CARs contain 3 activation motifs. The incorporation of 3 additional immune-based tyrosine activation motifs (ITAMs) into BBz CARs increases the latter's antigen sensitivity, albeit still not matching that of a 28z CAR, while the disruption of ITAMs in 28z CARs diminishes the latter's antigen sensitivity[22]. Under CAR stress test conditions, wherein low T cell doses are purposefully administered to stringently challenge CAR T cells in vivo[21,24-26], CAR T cells generally fail to control leukemia presenting with less than a few thousand CD19 molecules per cell[21], consistent with clinical studies reporting tumor relapses with reduced target antigen expression[10,11,16,27].

Cognizant of the high sensitivity of the T cell receptor (TCR) for HLA-peptide complexes,[28,29] we used *TRAC* locus editing[24] to establish in human primary T cells a novel antigen receptor structure incorporating into the TCR/CD3 complex the same heavy and light chains as those assembled into an scFv within a corresponding CAR. These receptors, termed HLA-independent TCRs or HIT receptors, are more sensitive than CD28-based CARs and open new prospects for the targeting of low-density antigens.

Results

Basic functions of a CD19-specific HIT receptor

To confer CD19 specificity to the TCR/CD3 complex, we targeted the *TRAC* locus[24] in human peripheral blood T cells to reconstruct the antigen binding domain of the heterodimeric TCR to match that of a CD19 CAR[14]. To generate the HIT receptor (Fig. 1a), the CAR heavy chain sequence was fused to that of the TCR Cβ domain ($V_HC\beta$), and the CAR light chain sequence to the genomic Cα sequence ($V_LC\alpha$), thus generating chimeric $V_HC\beta$ and $V_LC\alpha$ chains linked by a P2A element (Fig 1a) under the transcriptional control of endogenous TCR promoter and polyA elements. This genetic modification results in a substituted TCR specificity, replacing the HLA-restricted Vα-Vβ pair with HLA-independent CD19-specific V_L–V_H binding domains. The disruption of the endogenous *TRAC* locus ablated cell-surface CD3 expression, which remained undetected when knocking-in the 19-28z CAR[24], but was restored to the cell surface in cells engineered to express $V_HC\beta$ and $V_LC\alpha$ (Fig 1b and Extended Data Fig. 1a). T cells expressing either 19-28z (*TRAC*-CAR) or the $V_HC\beta$/ $V_LC\alpha$ heterodimer (*TRAC*-HIT) stained positively with the same polyclonal antibody used to detect the SJ25C1 scFv[30] in the 19-28z CAR[14] (Fig 1b and Extended Data Fig. 1a,b). *TRAC*-edited T cell populations specifically lysed CD19+ target cells, confirming the formation of an active CD19 HIT receptor, and did not lyse $CD19^-$ target cells (Fig 1c and Extended Data Fig. 2). Both *TRAC*-HIT and *TRAC*-CAR bound soluble CD19 protein with HIT T cells exhibiting lower overall binding capacity per cell compared to CAR T cells (Fig. 1d). Both CAR and HIT receptors elicited similar cytokine responses upon exposure to NIH 3T3 cells overexpressing CD19 (Extended Data Fig. 3a). Following repeated exposure to antigen, both receptors similarly internalized (Extended Data Fig. 3b) and maintained a similar CD4/CD8 T cell ratio in engineered peripheral blood T cells (Extended Data Fig. 3c).

Recognition of CD19 was not limited to the heavy and light chains of SJ25C1 and was likewise obtained with the variable chains of FMC63, another CD19-specific scFv[13,31] (Extended Data Fig. 1c), further supporting the structural compatibility of antibody and TCR Ig-like domains[32-34]. The HIT structure we report here differs from other recently reported HLA-independent, CD3-associated receptors[35-38], all of which retain their endogenous clonotypic TCR and thus generate dual-specific T cells. These other receptors either have scFvs fused to CD3 components[35] or interact with the endogenous TCR/CD3 complex[36], or are composed of IgV-TCRC chimeras comprising γδ[37] or mouse αβTCR[38] constant regions to avoid mispairing with endogenous TCR chains. Importantly, the HIT receptor design endows the T cell with a single specificity.

As the SJ25C1 and FMC63 CD19-specific scFvs have a similar, high affinity, we investigated an additional set of 3 CD19-specific scFvs, all specific for the same epitope but differing in their affinity (1.3, 4.9 and 32 nM, respectively). The paired *TRAC*-HIT and *TRAC*-CAR T cells similarly bound to soluble CD19 (Extended Data Fig. 4), but while the three 28z CARs directed comparable cytolysis of NALM6, the HIT receptors showed diminishing cytolysis with decreasing affinity (Fig 1e). This observation suggested that HIT receptors, which do not benefit from CD4 or CD8 co-receptors like typical TCRs, may operate differently from TCRs, which prompted us to evaluate whether HIT T cells could nonetheless respond to low antigen levels.

HIT receptors provide greater antigen sensitivity than CARs

To assess the antigen sensitivity of HIT receptors, we established a panel of NALM6 variants stably expressing a range of CD19 levels (Extended Data Fig. 4a-d). A striking difference between *TRAC*-HIT and *TRAC*-CAR T cells promptly emerged, showing that HIT T cells could lyse clones that 19-28z CAR T cells could not (Fig. 2). Both receptors were similarly effective against NALM6 and NALM6 variants expressing within 10-fold less CD19 than wild-type (WT) NALM6 (Fig. 2a,b and Extended Data Fig. 4f,g). As CD19 levels further decreased, *TRAC*-CAR T cells no longer killed their target, in contrast to *TRAC*-HIT T cells (Fig 2a,b and Extended Data Fig. 5f,g). We next quantified CD19 levels in a subset of NALM6 variants, identifying clones with 20-2,000 CD19 molecules, well below the count of 27,000 measured in parental NALM6 (Fig. 2c-d, and Extended Data Fig. 5e). *TRAC*-CAR T cells could effectively lyse NALM6 variants down to ~200 molecules per cell but not less, while *TRAC*-HIT T cells still effectively lysed clones with ~20 molecules per cell (Fig 2e). The same results were obtained with the V_H and V_L chains from either SJ25C1[14] or FMC63[13,31] (Extended Data Fig. 5f). Significantly, we compared HIT receptor sensitivity to the more sensitive 28z CARs (Ref.[22,23] and Extended Data Fig. 5g).

This observation was extended with another HIT receptor specific for CD22, constructed with variable chains taken from a CD22-specific CAR[9,21]. Both the CD19 and CD22 HIT receptors lysed MM1S (Extended Data Fig. 6), a BCMA-positive myeloma cell line displaying very low-level expression of those two antigens (confirmed by FACS analysis and quantitative mass spectrometry (Extended Data Fig. 6a,b), but not the CD19 or CD22-specific CARs. In contrast, both BCMA-specific CAR[10,21] and HIT receptors lysed MM1S (Extended Data Fig. 6c and Extended Data Fig. 2). Altogether, these results confirm that HIT receptors endow T cells with greater antigen sensitivity than canonical CARs.

This conclusion is further supported by the cytokine response of *TRAC*-HIT T cells elicited by low antigen density target cells. Expression of interferon-γ, interleukin-2 and tumour necrosis factor-α was 3 to 10-fold higher in both CD4 and CD8 T cells upon exposure to NALM6 cells expressing ~20 CD19 molecules per cell, compared to *TRAC*-CAR T cells (Fig. 2f). Above 200 CD19 molecules per cell, *TRAC*-CAR and *TRAC*-HIT T cells showed similar cytokine profiles (Fig. 2f).

We hypothesized that this increased sensitivity of HIT receptors is due to their greater signalling response and measured the phosphorylation of CD3ζ and ZAP70 and downstream ERK1/2.[39] HIT-engineered T cells indeed showed greater CD3ζ, ZAP70 and ERK1/2

phosphorylation upon exposure to the low antigen density NALM6/12-4 compared to *TRAC*-CAR T cells (Fig. 2g and Extended Data Fig. 7). This difference was even greater with antigen levels below 200 mol./cell (NALM6/7), where CAR T cells showed hardly any detectable pERK1/2 upon exposure to the CD19+ cells in contrast to HIT T cells (Fig. 2g and Extended Data Fig. 7). At higher antigen densities (NALM6/WT and NALM6/12-4), *TRAC*-HIT and *TRAC*-CAR T cells showed comparable levels of pERK1/2 and a similar percentage of pERK1/2 positive cells (Fig. 2h and Extended Data Fig. 7). In aggregate, these studies point to a threshold of about 200 CD19 molecules per cell for effective 19-28z CAR-mediated T cell activation *in vitro* while only ~20 molecules suffice for *TRAC*-HIT T cells.

HIT T cells display faster degranulation and cytotoxicity

To gain further insight into the mechanism for the HIT receptor's greater antigen sensitivity, we performed quantitative phospho-proteomic analyses of *TRAC*-HIT T cells when activated with low-antigen targets (NALM6/7), comparing their profile to *TRAC*-CAR T cells (Fig 3a). *TRAC*-HIT T cells showed a higher number of phospho-peptides after a 10-min incubation with NALM6/7 (Fig 3a), thus providing further support for their greater sensitivity to low antigen levels. Phospho-peptides with a $p<0.05$ ($-\log10>1.3$) detected in two independent experiments with different T cell donors were further analysed (Fig 3b). Applying a cut-off log2 ratio of 0.7, *TRAC*-HIT T cells showed enrichment of a set of phospho-peptides involved in T cell activation and actin remodelling (Fig 3b). These included signalling molecules such as CD3 epsilon, LAT, GRAP2, AHNAK, and SLAMF1[40-42] and proteins involved in actin remodelling (ARPC1B).[43]

These findings prompted us to analyse actin remodelling as well as lysosome localization in *TRAC*-HIT and *TRAC*-CAR T cells when exposed to high and low antigen levels. We specifically quantified the F-actin enrichment and LAMP-1 lysosomes at the immunological synapse (IS) in over 60 NALM6-T cell conjugates (2 different T cell donors). We observed no significant difference in F-actin enrichment between HIT and CAR T cells (Fig. 3c and Extended Data Fig. 8a) but found that CAR and HIT localization at the IS are dependent on the antigen level on the target cell (Fig. 3c and Extended Data Fig. 8a). HIT T cells showed a more uniform distribution of LAMP-1 lysosomes at the IS than CAR T cells (variance $p=0.0006$) when incubated with low-antigen NALM6/7 (Fig 3d), but not with high-antigen NALM6 (Extended Data Fig. 8a). We thus hypothesised that HIT T cells would be more proficient at degranulation than CAR T cells when exposed to low antigen levels. We assessed degranulation by measuring CD107a in T cells incubated for 1h and 4h with different NALM6 targets. *TRAC*-HIT T cells degranulated faster and significantly more frequently than *TRAC*-CAR T cells when incubated with NALM6 cells expressing ~ 20 molecules of CD19 (NALM6/7; Fig. 3e and Extended Data Fig. 8b,c). This difference vanished with antigen levels above 200 CD19 molecules (NALM6/12-4 and NALM6/WT; Fig. 3e and Extended Data Fig. 8b,c).

Based on the above observations on phospho-proteomics, lysosome mobilization and degranulation, we predicted that *TRAC*-HIT T cells will be more rapid than *TRAC*-CAR T cells at killing targets with low antigen levels. We therefore measured the time required

for target lysis kinetics by HIT and CAR T cells in single-cell conditions (1:1 T cell:target cell in single wells).[21] *TRAC*-CAR and *TRAC*-HIT T cells displayed similar kinetics when incubated with NALM6 WT and NALM/12-4 targets, but TRAC-HIT T cells were faster when exposed to NALM6/7 (Fig. 3f). Altogether, we conclude that HIT receptors impart increased antigen sensitivity to T cells by, at least in part, enabling greater mobilization and release of lytic granules than CARs in the context of low antigen density.

HIT T cells outperform CAR T cells against low-antigen tumours

We investigated the capacity of *TRAC*-HIT T cells to control tumours expressing different antigen levels *in vivo*. In a "stress test" setting, wherein we deliberately infuse sub-curative T cell doses to quantify and compare T cell potency,[21,24,26] we first compared *TRAC*-HIT T cells to first and second generation[5] *TRAC*-CAR T cells in controlling NALM6, a commonly investigated pre-B acute lymphoblastic leukemia.[21,24,26] Since the 28z CAR is more sensitive than BBz, BBzz and 28-1XX CARs[21-23], we focused on 28z CARs for comparison in our *in vivo* studies. Over the first 3 weeks, *TRAC*-HIT T cells vastly outperformed first-generation CAR T cells (19z1) and strikingly rivalled the second-generation CAR T cells, despite lacking engineered costimulation unlike the 1928z CAR (Fig 4a). The gap between *TRAC*-19z1 and CD19 *TRAC*-HIT, which both are activating receptors lacking embedded costimulatory domains, illustrates the greater efficacy of the CD3 complex relative to that of a ζ chain fusion receptor. When targeting a low abundance NALM6 variant (12-4), we observed superior tumour elimination by *TRAC*-HIT T cells, most notably in the first week ($p=0.002$, Fig 4b).

In considering the advantage afforded to the CAR by the incorporation of a costimulatory domain (Fig 4a) and the latter's absence in the HIT receptor, we tested the hypothesis that providing costimulatory support to *TRAC*-HIT T cells would enable the latter to further outperform the 1928z CAR by extending their persistence. To this end, we co-expressed ligands for CD28 and 4-1BB in the T cells, which we previously showed enhances the persistence of first[44] and second[26] generation CARs. Consistent with earlier findings[26,44,45], co-expression of these two ligands (annotated 80/BBL) increased the therapeutic potency of *TRAC*-HIT T cells, whereas co-expression of either ligand alone did not (Extended Data Fig. 9a). In two models, targeting either CD19 or BCMA, *TRAC*-HIT+80/BBL T cells yielded greater survival than 28z CAR T cells (Fig. 4c,d and Extended Data Fig. 10a,b).

In the NALM6/12-4 leukemia model, *TRAC*-19HIT+80/BBL outperformed *TRAC*-CAR T cells ($p=0.0001$, Fig. 4c). Furthermore, in the MM1S myeloma model, where BCMA is more abundant (~ 11,000 molecules per cell) than CD19 in NALM6/12-4 (~200), *TRAC*-BHIT+80/BBL T cells likewise outperformed *TRAC*-BCAR T cells ($p=0.048$, Fig. 4d). Thus, T cells expressing the HIT receptor alone provided sensitive tumour recognition but did not significantly prolong mouse survival until they were supported by 80/BBL-based costimulation (Fig. 4d and Extended Data Fig. 10c). Bone marrow analyses on days 10 and 17 showed that the improved early tumour control obtained in *TRAC*-HIT compared to *TRAC*-CAR treated animals was not the result of increased T cell numbers. CD4 and CD8 *TRAC*-HIT T cells were present in similar numbers to *TRAC*-CAR T cells on day 10 and less abundant by day 17 (Extended Data Fig. 9b,c). *TRAC*-HIT+80/BBL T cells on the other

hand exceeded *TRAC*-HIT and *TRAC*-CAR T cells at both time points. Altogether, these *in vivo* studies establish that T cells reprogrammed with a HIT receptor display greater in vivo antigen sensitivity than a CAR, and that prolonged tumour control by HIT T cells can be achieved by providing supportive cell-intrinsic costimulation.

We provide an additional example targeting another clinically relevant target of low abundance, CD70 in acute myeloid leukaemia (AML). [46,47] We utilized the AML cell line MOLM13 which is derived from FLT3-ITD relapsed AML and expresses ~370 CD70 molecules per cell based on *ex vivo* bone marrow analysis (Fig 4e). 70HIT and 70CAR T cells effectively lysed CD70+ MOLM13 in vitro (Fig 4f) but not $CD70^{-}$ target cells (Extended Data Fig. 2). However, neither CAR nor HIT T cells were effective *in vivo* (Fig. 4g and Extended Data Fig. 10e). CD70 expression is induced in activated T cells and high CD70 levels are detectable in a sizable fraction of CAR-transduced T cells (Ref[48] and Extended Data Fig. 10d), which may result in HIT/CAR-mediated fratricide T cell killing and/or HIT/CAR malfunction when targeting CD70. We therefore ablated CD70 expression in the infused T cells (Extended Data Fig. 10d) and found that anti-AML efficacy was indeed improved. In this instance again, 70HIT+80/BBL T cells vastly outperformed the CAR T cells ($p<0.0001$, Fig. 4g and Extended Data Fig. 10e).

Discussion

A general comparison of CARs and TCRs is rendered difficult by the multiplicity of CAR structures and the distinct nature of their respective ligands (various cell surface molecules vs HLA-peptide complexes). Nonetheless, the HIT design reported here allows to examine a TCR-like structure and a CAR that engage the same target using the same heavy and light immunoglobulin chains. CARs and HIT receptors both direct effective killing of target cells that express thousands of target molecules. However, as the target antigen numbers diminish to the hundreds, the HIT receptor exceeds the antigen sensitivity afforded by CARs, including the more sensitive CD28-based CARs. This difference allows, as we show here, for HIT-engineered T cells to reject tumours that CAR T cells struggle to control. Based on in vitro cytolysis experiments, HIT receptors are at least 10-fold more sensitive to antigen than CARs. This heightened sensitivity is consistent with that attributed to the physiological TCR/CD3 complex. *In vitro* studies suggest that TCRs only require 1-3 ligands to be engaged for cytolysis,[28,29] but the number of required TCR ligands for effective *in vivo* tumour elimination is less well defined (one study calculated that 30-60 ligands per cell would be required to support T cell expansion[49,50]). Future studies are needed to better quantify threshold antigen levels required for effective CAR, HIT and TCR based therapies.

We found that *TRAC*-HIT T cells can lyse target cells with low antigen density and that their degranulation and lytic kinetics are greater than those of CAR T cells when antigen is limiting. Our phospho-proteomic and morphological studies support a mechanism whereby HIT engagement is more effective in remodeling actin or recruiting lysosomes. This may entail the activation of ARPC1B, which is necessary for the establishment of lamellipodia as well as the actin reorganization required for cell migration and immune synapse formation.[43] Our analyses also point to signaling differences that underpin differential antigen sensitivity,

such as the activation of LAT, which our study and another suggest is poorly recruited by CARs.[51] The HIT vs CAR system we describe here is poised to provide many more future insights into CAR and HIT functions. More quantitative and sensitive techniques are still needed to accurately quantify receptor expression, measure receptor affinities, early signaling events and the dynamic structure of the immune synapse, as are structural studies to determine how CAR and HIT receptors engage their cognate target.

Heavy and light chains have been previously used in the context of T cell receptors through different means.[35-38] However, their antigen sensitivity or their ability to exert tumor control has not been evaluated against low antigen density tumours[35-37] other than for the STAR receptor.[38] In all these instances,[35-38] T cells were dual-specific as they retained their endogenous TCR and expressed the VL-VH fusion proteins from randomly integrated lentiviral vectors. Dual specificity may impact antigen sensitivity, as the VL and VH fusion proteins compete with endogenous αβTCR chains or assembly with CD3 complex components. Amongst these receptors, the STAR receptor[38] is the only one reported to have increased sensitivity compared to 28z and BBz CARs, in line with our observations, although the minimal number of target molecules needed to trigger T cell activation has not been addressed. The HIT receptor design minimizes competition with the endogenous TCR through the disruption of the TCRα, provides homogenous HIT receptor expression from the *TRAC* locus and abrogates T cell alloreactivity.

As we show here, HIT receptors enable effective recognition targeting of low antigen density targets but they require additional support to enhance their therapeutic efficacy. Unlike second generation CARs[4,5], HIT receptors are not endowed with costimulatory components, but costimulatory support can be engineered separately into the T cell, as previously established with other antigen receptors[26,44,52,53] and extended in this study. Given the similarity of HIT receptors and TCRs, our findings provide a strong rationale for similarly endowing TCR-engineered and natural T cells with generic costimulatory support, e.g. via constitutive CD80 and 4-1BBL co-expression, to increase their persistence and potency.

The different activation and therapeutic thresholds of TCRs, HITs and CARs open new possibilities for cancer immunotherapy. CARs are effective against high density antigens and may have reduced potential to damage normal tissues that express sub-threshold levels of the targeted antigen. This therapeutic window however raises the risk of escape of low-expressor tumour cells. HIT receptors, on the other hand, are better suited for targets expressed in the lower ranges, as exemplified here in our in vivo models targeting CD19 and CD70. HIT receptors will be especially valuable against tumour-specific targets of low abundance, for which the risk of reactivity against normal tissues expressing the antigen is averted by default, or when paired with another receptor in an "*and*" gate. *TRAC*-HIT T cells should thus expand the realm of tumours that can be targeted by engineered T cells.

Methods

All animal research complies with the ethical regulations from the MSKCC Institutional Animal Care and Use Committee.

Data reporting.

The experiments were not randomized, and the investigators were not blinded to allocation during experiments and outcome assessment, except where noted.

Guide RNA.

The sequence targeted by *TRAC* gRNA is located upstream of the transmembrane domain of the TCRα.[6] *TRAC* gRNA target sequence: 5′-CAGGGTTCTGGATATCTGT. *CD70* gRNA target sequence: 5′- GGGCTTGGTGATCTGCCTCG. *TRAC* and *CD70* gRNAs were ordered from Synthego with 2′-O-methyl 3′ phosphorothioate modifications in the first and last 3 nucleotides[54]. Guide RNA was resuspended with TE buffer at 40 μM.

Cas9 protein and RNP formation.

Cas9 protein (40 μM) was obtained from QB3-Berkeley Macrolab core facility. *TRAC* RNP was prepared by mixing Cas9 protein and *TRAC* gRNA at 1:1 molar ratio and incubated at 37 °C for 15 min, and immediately used for T cell targeting experiments.

AAV.

We designed and cloned the pAAV-*TRAC*-19HIT by replacing the 1928z-polyA sequence of our previously described pAAV-*TRAC*-1928z plasmid.[6] To express a HIT receptor at the *TRAC* locus, the V_H-Cβ-P2A-V_L sequence is cloned in between of the P2A and the *TRAC* exon1 elements (chimeric V_H-Cβ and V_L-Cα (exon1) sequences are provided in Supplementary Information), thus resulting in V_H-Cβ and V_L-Cα expression under the control of TCRα promoter. CD19-specific HITs are generated using V_H and V_L elements derived from the SJ25C1 or FMC63 CAR genes previously described[23] or from 3 human scFvs of different affinities that recognize the same epitope (a kind gift of Ken Mohler from Juno Therapeutics). HIT V_H and V_L sequences used to produce CD22- and BCMA-specific HITs are derived from previously described CAR genes.[23] *TRAC*-1928z and *TRAC*-19BBz as in ref. 6; *TRAC*-1928z1, *TRAC*-2228z, and *TRAC*-BCMA28z were cloned by replacing 1928z in the *TRAC* AAV construct with the 19z1,[25] 2228z,[23] and BCMA28z[23] sequences. Recombinant AAV6 viruses (with AAV2 ITRs) were produced by Vigene, with titers expressed as GC/ml.

Lentiviral vector construction, production, and transduction.

PGK100-CD19 lenti plasmid was generated by cloning the PGK100 promoter[6] and CD19[23] sequences into a SIN lentiviral plasmid (pLM backone)[55]. VSV-G pseudotyped lentiviral supernatants derived from transfected 293T cells were used to transduce NALM6/12 cells (see below) to generate stable NALM6 cells expressing CD19 at very low levels. Transduction was performed in 6-well plates containing 4 ug/ml polybrene. Cells with less than 5% transduction efficiency were used to clone the new CD19-expressing NALM6 clones by limited dilution in round bottom 96-well plates.

Gammaretoviral vector construction, production, and transduction.

Plasmids encoding the SFGγ retroviral vector[56] were used to clone the bicistronic construct to express human CD80[25] and 41BBL[25] genes. CD80 and 41BBL SFGγ retroviral vectors

have been previously described.[25] Vesicular stomatitis virus glycoprotein G (VSV-G) pseudotyped retroviral supernatants derived from transduced gpg29 fibroblasts (H29) were used to construct stable retroviral-producing cell lines[33]. T cells were transduced with retroviral supernatants by centrifugation on RetroNectin-coated plates (Takara), as described previously.[6] CD80 and 41BBL expression was detected by FACS using mouse anti-human CD80-PE and 41BBL-PE antibodies (BD).

Cell lines.

Firefly-luciferase (FFL)-expressing NALM6 cells and CD19-expressing NIH/3T3 cells were cultured as described (Eyquem et al). NALM6/Medium and NALM6/Low cell lines (~10,000 and ~,1500 molecules per cell, respectively) were previously described.[23] CRISPR/Cas9-edited NALM6 cells were generated as described, [23] and cloned using the limited dilution technique. NALM6 clones with very low CD19 levels were selected for this study. NALM6/12-4 and NALM6 /12-39 are derivatives of clone NALM6/12, which was transduced with the PGK100-CD19 lentivector as described above. All NALM6 cell lines were maintained in RPMI 1040 medium supplemented with 10% fetal bovine serum (FBS; HyClone), 10 mM HEPES (Invitrogen), 2 mM L-glutamine (Invitrogen), 1X NEAA (Invitrogen), 1 mM sodium pyruvate (Invitrogen), 50 μM β-mercaptoethanol, 10U/ml Penicillin, 10 μg/ml Streptomycin (Gibco), and 2.5 μg/ml Plasmocyn (InvivoGen). Cells were split every 2-3 days and plated at $0.5x10^6$ cells/ml. Multiple myeloma cell line MM1S expressing FFLuc-mCherry (a kind gift of D. Maria Themeli) was cultured in RPMI 1040 medium supplemented with 10% fetal bovine serum (FBS; HyClone FetalClone I), 2 mM L-glutamine (Invitrogen), 1 mM sodium pyruvate (Invitrogen), 10 mM HEPES (Invitrogen), 10U/ml Penicillin, 10 μg/ml Streptomycin (Gibco), and 2.5 μg/ml Plasmocyn (InvivoGen). Cells were split every 2-3 days and plated at $1x10^6$ cells/ml. Acute myeloid leukemia cell line MOLM13 (a kind gift of Dr. Marion Subklewe) were transduced with FFLuc-GFP retroviral vector and further sorted (gated on GFP+ fraction). FFLuc-GFP-MOLM13 cells were cultured in RPMI 1040 medium supplemented with 10% fetal bovine serum (FBS; HyClone FetalClone I), 2 mM L-glutamine (Invitrogen), 10U/ml Penicillin, and 10 μg/ml Streptomycin (Gibco). Cells were split every 2-3 days and plated at $0.5 x10^6$ - $2x10^6$ cells/ml.

CD19, BCMA, and CD70 quantification.

NALM6 cells ($0.2x10^6$), MM1S cells ($0.1x10^6$), and *in-vitro* and *ex-vivo* MOLM13 cells ($1x10^6$) were stained with 5 ul PE-anti CD19 antibody (clone SJ25C1, BD), 10 ul PE-anti BCMA antibody (clone 19F2, Biolegend), and 4 ul PE-anti-CD70 antibody (clone 113-16, Biolegend), respectively, in 100 ul MACS buffer for 30 min at 4 °C, washed and analysed by FACS. Phycoerythrin Fluorescence Quantitation Kit (BD) was used according to the manufacturer's protocol to determine the number of CD19, BCMA, and CD70 molecules per cell. To quantify CD19 in NALM6/2, NALM6/7, NALM6/12, CD19 gMFI were used to calculate a ratio with NALM6/12-4 CD19 gMFI. Based on the number of CD19 molecules determined for NALM6/12-4, the ratios were used to calculate the number CD19 molecules per cell in the aforementioned cell lines.

Quantitative mass spectrometry.

NALM6 and MM1S cell pellets (~4 million cells) were lysed in 8 M Urea, 200 mM EPPS (4-(2-Hydroxyethyl)-1-piperazinepropanesulfonic acid), pH 8.5 with protease (complete mini EDTA-free, Roche) and phosphatase inhibitors (cocktail 2 and 3, Sigma). Samples were then sonicated (Diagenode Bioruptor) for 3 cycles [1 min ON/1 min OFF]. The BCA assay was then used to determine the protein concentrations. Aliquots of 100 μg were taken for each sample (based on BCA assay) and reduced with 5 mM TCEP (tris(2-carboxyethyl)phosphine hydrochloride), alkylated with 10 mM IAA (iodoacetamide), and quenched with 10 mM DTT (dithiothreitol). Samples were diluted to about 100 μL with lysis buffer and precipitated by chloroform-methanol[57]. Pellets were resuspended in 50 μL 200 mM EPPS buffer, digested with Lys-C protease at a 1:50 protease-to-protein ratio for 5 hours at 37°C, then overnight with trypsin (1:50) at 37°C.

Anhydrous acetonitrile was added at a final volume of 30%. TMTPro (16-plex) reagents were added to peptides at a 2.8:1 (TMT reagent-to-peptide ratio) and incubated for 1 hour at room temperature. A label check was performed to determine mixing ratios, labelling efficiency, and number of missed cleavages by pooling 1 ug from each sample, desalting, then analysing by mass spectrometry. Samples were mixed 1:1 across all channels, dried to remove acetonitrile, then desalted using C18 solid-phase extraction (SPE) Sep-Pak (Waters), and vacuum centrifuged to dryness.

Peptides were reconstituted in 1mL of 2% ACN/25 mM ABC and fractionated into 48 fractions. Briefly, an Ultimate 3000 HPLC (Dionex) coupled to an Ultimate 3000 Fraction Collector using a Waters XBridge BEH130 C18 column (3.5 um 4.6 x 250 mm) was operated at 1mL/min. Buffer A consisted of 100% water, buffer B consisted of 100% acetonitrile, and buffer C consisted of 25 mM ABC. The fractionation gradient operated as follows: 1% B to 5% B in 1 min, 5% B to 35% B in 61 min, 35% B to 60% B in 5 min, 60% B to 70% B in 3 min, 70% B to 1% B in 10min, with 10% C the entire gradient to maintain pH. The 48 fractions were then concatenated to 12 fractions (i.e. fractions 1, 13, 25, 37 were pooled, followed by fractions 2, 14, 26, 38, etc.) so that every 12^{th} fraction was used to pool. Pooled fractions were vacuum-centrifuged then reconstituted in 1% ACN/0.1% FA for LC-MS/MS.

Fractions were analysed by LC-MS/MS using a nanoAQUITY UPLC (Waters) with a 50 cm (inner diameter 75μm) EASY-Spray Column (PepMap RSLC, C18, 2μm, 100Å) heated to 60°C coupled to a Orbitrap Fusion Lumos Tribrid Mass Spectrometer (Thermo Fisher Scientific). Peptides were separated at a flow rate of 300nL/min using a linear gradient of 1 to 35% acetonitrile (0.1% FA) in water (0.1% FA) over 4 hours and analysed by SPS-MS3. MS1 scans were acquired over a range of m/z 375-1500, 120K resolution, AGC target of $4x10^5$, and maximum IT of 50 ms. MS2 scans were acquired on MS1 scans of charge 2-7 using an isolation of 0.7 m/z, collision induced dissociation with activation of 35%, turbo scan and max IT of 50 ms. MS3 scans were acquired using specific precursor selection (SPS) of 10 isolation notches, m/z range 100-1000, 50K resolution AGC target of $1x10^5$, HCD activation of 65%, and max IT of 150 ms. The dynamic exclusion was set at 38 s.

Raw data files were processed using Proteome Discoverer (PD) version 2.4.0.305 (Thermo Scientific). For each of the TMT experiments, raw files from the all fractions were merged and searched with the SEQUEST HT search engine with a *Homo sapiens* UniProt protein database downloaded on 2019/01/09 (176,946 entries). Methionine oxidation was set as variable modification, while Cys carbamidomethylation, TMT16plex (K) and TMT16plex (N-term) were specified as fixed modifications. The precursor and fragment mass tolerances were 10 ppm and 0.6 Da respectively. A maximum of two trypsin missed cleavages were permitted. Searches used a reversed sequence decoy strategy to control peptide false discovery rate (FDR) and 1% FDR was set as threshold for identification.

T cell isolation, activation, and culture.

Buffy coats from healthy volunteer donors were obtained from the New York Blood Center. Peripheral blood mononuclear cells were isolated by density gradient centrifugation, and typically frozen in 90% FBS /10% DMSO. Frozen PBMCs were cultured for 1h in T cell medium (see below; >85% viability) and then used for T cell isolation. T lymphocytes were purified using the Pan T cell isolation kit (Miltenyi Biotech). T cells (>90% viability) were activated with Dynabeads (1:1 beads:cell) Human T-Activator CD3/CD28 (ThermoFisher) in X-vivo 15 medium (Lonza) supplemented with 5% human serum (Gemini Bioproducts) with 5 ng/ml human recombinant IL7 (Peprotech) and 5 ng/ml human recombinant IL15 (Peprotech) at a density of 10^6 cells per ml. The medium was changed every 2 days, and cells were replated at 1-1.5 $x10^6$ cells per ml.

Gene editing and targeting.

Forty-eight hours after initiating T-cell activation, the CD3/CD28 beads were magnetically removed, and the T cells were cultured for an extra day. T cells were transfected by electrotransfer of *TRAC* RNP using the Nucleofector II device (Lonza). $2x10^6$ or $10x10^6$ cells were resuspended with P3 buffer (Lonza) and mixed with 60 or 300 pmoles *TRAC* RNP in a total volume of 20 or 100 µl, respectively. Following electroporation and considering 66.7% viability, cells were diluted into culture medium at $1x10^6$ cells per ml, and incubated at 37 °C, 5% CO_2. Recombinant AAV6 donor vector was added to the culture 30min-1h after electroporation, at a multiplicity of infection of $3x10^5$ GC per cell. Subsequently, edited cells were cultured using standard conditions (37 °C and expanded in T-cell growth medium, replenished as needed to maintain a density of 1-1.5$x10^6$ cells per ml every 2 days). For the generation of CD70-targeting CAR T cells, T cells were electroporated with *TRAC* and *CD70* RNPs, followed by AAV transduction (70HIT T cells) or SFGγ-retroviral vectors (70CAR T cells), immediately or 20-24h post-electroporation, respectively.

Multiple antigen-stimulation assay.

NIH/3T3 expressing human CD19 were used as artificial antigen-presenting cells as described.[6] For repeated proximal stimulations, single-stimulation cells were transferred to a new well plated with CD19+ NIH/3T3 after 24 h (2 stimulations) or every 12 h (4 stimulations). For each condition, T cells were counted and analysed by FACS for HIT and CAR every 12h and CD4, CD8 and differentiation markers (CD45RA and CD62L) expression at the end of the experiment (48h).

Cytotoxicity assays.

The cytotoxicity of *TRAC*-HIT and *TRAC*-CAR T cells was determined by standard firefly luciferase (FFL)-based assay.[6] FFL-expressing NALM6, PC3, or MM1S served as target cells. The effector (E) and tumour target (T) cells were co-cultured in duplicates at the indicated E/T ratio using black-walled 96-well plates with $1x10^5$ target cells in a total volume of 100 µl per well in T cell medium. Four or 18 h later, 100 µl luciferase substrate (Bright-Glo, Promega) was directly added to each well. Emitted light was detected in a luminescence plate reader, and lysis was calculated using the formula 100 x (1-(RLUsample)/(RLUtarget alone)).

Single-cell cytotoxicity assayd.

TRAC-HIT and *TRAC*-CAR T cells were stimulated once with CD19+ NIH/3T3 cells as described above, and expanded for 1 week in T cell medium. The day before the assay was started, HIT and CAR expression were quantified by FACS. Single cell CTL assays were performed as described.[23] In brief, chamber slides containing a micro-well grid (50 × 50 × 50 µm per well) were loaded with 1 × 10 CellTrace Violet-containing HIT^+/CAR^+ T cells, along with with unlabelled NALM6 cells at a ratio of 1:1 in the presence of 1.5 µM of propidium iodide (PI, Life Technologies). Images were acquired with an AxioObserver.Z1 microscope (Carl Zeiss) using 20×/0.5 or 40×/0.6 objectives. Fifteen positions (1 position = 36 micro-wells) for each chamber were imaged every 10 min for 24 h. Acquired images were processed using a custom macro written on ImageJ software. Each individual well was scanned for the presence of T cells (CellTrace Violet). These wells were then analysed to identify wells containing a one effector (E) T cell and one single target (T) cell, and interactions were recorded. In wells in which conjugate formation led to target death (lytic conjugates; PI-positive wells), the duration of interaction between E:T was recorded from the formation to the interruption of the conjugate. Contact events lasting for only 1 frame (10 min) were not included. All analyses were performed in a blinded fashion.

Cytokine analyses.

To measure intracellular levels, $1x10^6$ *TRAC*-HIT or *TRAC*-CAR T cells were incubated with NALM6 targets at 1:1 ratio for 4h in the presence of Brefeldin A. T cells were fixed and permeabilized using BD Cytofix/ Cytoperm Plus kit as per the recommendation of the manufacturer, followed by staining with anti-cytokine antibodies (Brilliant Violet 785™ anti-human TNF-α Antibody (clone MAb11, cat# 502948, Biolegend; Brilliant Violet 421™ anti-human IFN-γ Antibody (clone B27, cat # 506538, Biolegend; PE anti-human IL-2 Antibody, (clone MQ1-17H12, cat# 500307, Biolegend; BUV395 Mouse Anti-Human CD4 (Clone SK3, cat# 563550, BD bioscience; BV711 Mouse Anti-Human CD45 (Clone HI30, cat #, BD bioscience; Fixable Viability Stain 510 (cat# 564406, BD bioscience) is used to excluded dead cells). Cytokine levels were determined by FACS.

To measure secreted cytokine levels, $0.5x10^6$ *TRAC*-HIT or *TRAC*-CAR T cells were incubated with $0.3x10^6$ CD19+ NIH/3T3 cells per well in a 24-well plate at 37 °C for 24h. Supernatant were collected and cytokines were quantified using BD Cytometric Bead Array kits (IL2-558270; IFNγ-560111; TNFα-560112) and flow cytometry.

Intracellular phosphoprotein analyses.

TRAC-HIT and *TRAC*-CAR T cells were stained with Fixable Viability Dye eFluor 506 (eBioscience 65-0866-14) and rested for 30 minutes in standard tissue culture conditions. *TRAC*-HIT or *TRAC*-CAR T cells were incubated with Nalm6 target cells for 15 minutes at a *TRAC*-HIT/CAR T cell-to-target ratio of 1:2. After antigen stimulation, the cells were fixed with Phosflow Fix Buffer I (BD 557870). Fixed cells were stained for the HIT/CAR with AF647-GAM, followed by 2% mouse serum (15 min at 4 °C), and subsequently permeabilized with Phosflow Perm Buffer III (BD 558050) following the manufacturer's procedure. Permeabilized samples were stained with antibodies detecting phosphorylated CD3ζ ITAM3 (pY142; BD 558448), ZAP70 (pY319; BD 557881) and ERK1/2 (pT202/pY204; BioLegend 369506).

CD19 binding assays.

CAR/HIT T cells were incubated in 100ul MACS buffer containing increasing concentrations of recombinant hCD19-hFc (R&D Systems, CF 9269-CD-050), at 4 °C for 60min. After a wash with 2ml of MACS buffer, cells were resuspended in 100ul MACS buffer containing anti-human IgG-PE (1:100 dilution), and further incubated for 30 min at 4C for 30min. Then, cells were washed as above, spun down, resuspended in 300 ul MACS buffer, and analyzed by FACS.

Cell stimulation and staining for CD107a expression.

To measure degranulation in response to target cell stimulation, effector cells were incubated with target cells at a 1:1 ratio. CD107a (APC) antibody was added to culture before stimulation. Unstimulated cells were incubated without target cells to detect spontaneous expression of CD107a. Cells were incubated at 37°C in 5% CO_2 and analyzed at two different timepoints: 1 hour and 4 hours. The cells were washed twice with PBS and stained using conjugated antibody, CD45 (BV650) for 15 minutes at room temperature. Next, the cells were washed and fixed using Cytofix Fixation kit according to manufacturer's protocol (BD Biosciences) and analyzed on the Aurora flow cytometer (Cytek, USA).

Flow cytometry.

CD19- and BCMA-specific HIT and CAR expression was measured with Alexa-Fluor-647-conjugated goat anti-mouse F(ab')2 antibody (AF647-GAM, Jackson ImmunoResearch, 115-606-003). CD22-specific HIT and CAR expression was measured with biotinylated protein L (Thermo Scientific) followed by BV510–streptavidin (BD). TCRαβ was detected with mouse anti-human TCRαβ-FITC (Miltenyi Biotec). For T cell phenotyping the following antibodies were used: mouse anti-human BUV-395-CD4 (563552), APC- cy7-CD8 (557834), BB-515 CD45RA clone HI100 (RUO, 564552), BV-421-CD62L (563862), BV-510-CD279 (PD1, 563076) from BD biosciences; FITC-CD45RA (11-0458-42), PerCP-eFluor710-CD223 (LAG-3, 46-2239-42) from eBiosciences and FITC mouse anti-human CD366 (TIM-3, 345032) from Biolegend. The phenotype of primary cells and cell lines was determined using the following anti-human antibodies: CD19–PE (clone SJ25C1, BD), CD22–PE (clone S-HCL-1, BD), BCMA–BV421 (clone 19F2, BD), CD3–BUV737 (clone UCHT, BD), PD-1–BV711 (clone EH121, BD), LAG-3–BV650 (clone 11C3C65,

Biolegend), TIM-3–BV785 (clone F38-2E2, Biolegend), CD45–BV711 (clone HI30, BD). Countbright beads (Invitrogen) were used to determine the absolute number of cells according to the manufacturer's protocol. 7-AAD or DAPI was used to exclude dead cells. For fixed cells, eFluor506 fixable viability dye (eBioscience) was used. Fc Receptor Binding Inhibitor Antibody Human (eBioscience) and Fc block Mouse (Miltenyi) were used to block Fc receptors. For degranulation studies, CD107a was measured in CD45+ cells by using anti-human CD45-BV650 (Biolegend, clone HI30) and anti-human CD107a-APC (Biolegend, clone H4A3) antibodies. Flow cytometric data were acquired on a 5-laser Aurora (Cytek Biosciences) or BD LSR-II, and analysed in FlowJo v10.1 (BD) or FCS Express 7 Flow (De Novo Software).

Quantitative phosphoproteomic analysis.

NALM6/7 cell line was cultured for at least one week in the presence of heavy amino acids as described.[21] For each replicate, 20 millions NALM6/7 were incubated with 20 millions CAR/HIT T cells for 10 min at 37°C, and immediately washed with cold PBS, centrifuged, and frozen in dry-ice. Cell pellets were lysed with 300 μL buffer containing 8M urea and 200mM EPPS (pH at 8.5) with protease inhibitor (Roche) and phosphatase inhibitor cocktails 2 and 3 (Sigma). Benzonase (Millipore) was added to a concentration of 50u/mL and incubated (RT, 15min) followed by sonication (Covaris) for 4 cycles [30 sec ON/30 sec OFF] at 4°C. Samples were centrifuged at 4°C, 14,000 g's for 10 min and supernatant extracted. The Pierce bicinchoninic acid (BCA) protein concentration assay was used for determining protein concentration. Protein disulfide bonds were reduced with 5 mM tris (2-carboxyethyl) phosphine (room temperature, 15 min), then alkylated with 10 mM iodoacetamide (RT, 30 min, dark). The reaction was quenched with 10 mM dithiothreitol (RT, 15 min). Equivalent volumes of lysate aliquots were taken for each sample (100 – 200 ug in each sample) and diluted to approximately 100 μL with lysis buffer. Samples were subject to chloroform/methanol precipitation as previously described[1]. Pellets were reconstituted in 50μL of 200mM EPPS buffer and digested with Lys-C (1:50 enzyme-to-protein ratio) and incubated at 37°C for 4 hours. Trypsin was then added (1:50 enzyme-to-protein ratio) and digested for 37°C overnight. Anhydrous acetonitrile was added to make a final volume of 30% ACN. Samples were TMT-labeled as described[1]. Briefly, samples were TMT-tagged by adding 10 μL (20 ug/uL) TMT or (28 ug/μL) TMTPro reagents for each respective sample and incubated for 1 hr (RT). A ratio check was performed by taking a 1μL aliquot from each sample and desalted by StageTip method[2] to confirm labeling efficiency. TMT-tags were then quenched with hydroxylamine to a final concentration of 0.3% for 15 min (RT). Samples were pooled in their entirety then vacuum-centrifuged to dryness. Dried samples were reconstituted in 1mL of 3% ACN/1% TFA, desalted using a 100mg tC18 SepPak (Waters), and lyophilized overnight. Phosphopeptides were enriched using the Thermo High-Select Fe-NTA Phosphopeptide Enrichment Kit (Cat. No.: A32992). The phosphopeptide elute was vacuum centrifuged to dryness and reconstituted in 100 μL of 1% ACN/25mM ammonium bicarbonate (ABC). A StageTip was constructed by placing two plugs with a narrow bore syringe of a C18 disk (3M Empore Solid Phase Extraction Disk, #2315) into a 200μL tip (VWR, Cat. #89079-458). StageTips were conditioned with 100 μL of 100% ACN, 70% ACN/25mM ABC, then 1% ACN/25mM ABC. Phospho-enriched sample was loaded onto the StageTip and eluted into 6 fractions of 3, 5, 8, 10, 12,

and 70% ACN/25mM ABC with 100 μL each. Fractions were immediately dried down by vacuum-centrifugation and reconstituted in 0.1% formic acid (FA) for LC-MS/MS. Phospho-enriched fractions were analyzed by LC-MS/MS using a NanoAcquity (Waters) with a 50cm EASY-Spray Column (PepMap RSLC, C18, 2μm, 100Å, 75μm I.D.) heated to 60°C coupled to a Orbitrap Eclipse Tribrid Mass Spectrometer (Thermo Fisher Scientific). Peptides were separated by direct inject at a flow rate of 300nL/min using a gradient of 5 to 30% acetonitrile (0.1% FA) in water (0.1% FA) over 3 hours then to 50% ACN in 30min and analyzed by SPS-MS3. MS1 scans were acquired over a range of m/z 375-1500, 120K resolution, AGC target (standard), and maximum IT of 50ms. MS2 scans were acquired on MS1 scans of charge 2-7 using an isolation of 0.5m/z, collision induced dissociation with activation of 32%, turbo scan and max IT of 120ms. MS3 scans were acquired using specific precursor selection (SPS) of 10 isolation notches, m/z range 110-1000, 50K resolution, AGC target (custom, 200%), HCD activation of 65%, and max IT of 150ms. The dynamic exclusion was set at 60s. Raw data files were processed using Proteome Discoverer (PD) version 2.4.1.15 (Thermo Scientific). For each of the TMT experiments, raw files from all fractions were merged and searched with the SEQUEST HT search engine with a Homo sapiens UniProt protein database downloaded on 2019/01/09 (176,945 entries). Cysteine carbamidomethylation was specified as fixed modifications, while Methionine oxidation, acetylation of the protein N-terminus, TMT6plex/TMTpro (K) and TMT6plex/TMTpro (N-term), phosphorylation (STY), label13C(6) (K) and label13C(6)15N(4) (R) were set as variable modification. The precursor and fragment mass tolerances were 10 ppm and 0.6 Da respectively. A maximum of two trypsin missed cleavages were permitted. Searches used a reversed sequence decoy strategy to control peptide false discovery rate (FDR) and 1% FDR was set as threshold for identification. Phosphosite localization was assigned by PD IMP-ptmRS node. Phosphopeptides without heavy labels measured in all replicates were log2-transformed and plotted. Another search using PD 2.4.1.15 also performed to check common phosphor peptides between experiment 1 and experiment 2 with only searching for light labeled amino acids. By applying filter log2FC > 0.75 and p-value <0.05, 2 phosphopeptides (from LAT and ARPC1B) are newly identified and these peptides were manually checked in Thermo XCalibur using m/z, retention time and charge state to confirm PD results.

Quantification of F-actin, LAMP-1 (lysosome), and CAR/HIT receptor at the immunological synapse.

12 mm ø coverslips (VWR; 631–0666) were washed with 70% ethanol and pre- coated with 0.02% of poly-l-lysine (Sigma–Aldrich; P8920) for 20 min at room temperature and were washed three times in water before being dried. NALM6 and CAR/HIT T cell were resuspended at a concentration of 2×10^6 cells/ml in complete medium. 100 000 cells of each cell type were added in an Eppendorf and the final volume was resuspended to mix the cells before being added on the coverslips for 30min at 37°C 5%CO2 for conjugate formation. Coverslips were washed once with cold PBS before fixation. Cells were fixed with 4% paraformaldehyde (Life Technologies; FB002) for 10 min at room temperature, washed once in PBS and excess of paraformaldehyde was quenched for 10 min with PBS 10 mM glycine (Thermo Fisher Scientific; G8898). Cells were permeabilized for 30 min at room temperature with PBS 0.2% bovine serum albumin (BSA; Euromedex; 04-100-

812) 0.05% Saponin (Sigma–Aldrich; S4521). Primary antibodies were added in the same buffer for 1h at room temperature: anti-LAMP1 (abcam, ab24170), goat anti-mouse Alexa Fluor 647, Alexa Fluor 546 phalloidin (Thermo Fisher; A22283). Cells were washed three times in permeabilization buffer and then incubated at room temperature for 30 min in the same buffer with a goat anti-rabbit coupled to Alexa Fluor 405 (life technologies A31556). After washing once with PBS BSA Saponin, and once with PBS, coverslips were soaked three times in PBS, three times in water, and mounted with 4–6 μl of Fluoromount G (SouthernBiotech; 0100–01) on slides (KNITTEL Starfrost) and dried overnight protected from light before microscope acquisition. Images were acquired with a Leica DmI8 inverted micro- scope equipped with an SP8 confocal unit using a 63× (1.4NA) objective. Z-stack images were acquired. Actin/GAM synaptic enrichment and lysosomes polarity were analyzed in Fiji and ImageJ softwares using scripts generated for semi-automated analysis.

In a first part, single images corresponding to the median plane of each conjugate was extracted from the Z-stacks. T cells were cropped and oriented in the same way regarding their synapse as described.[58] In a second part, after synapse extraction, for each crop, a mask of the T cell, the target cell and of the lysosomes were obtained after applying a threshold on the GAM, actin and Lamp1 channels respectively.

To obtain the contact zone corresponding to the synapse, the target cell was enlarged and the overlapping region with the T cell mask was selected and skeletonized. To define lysosomes polarity, a distance map showing the distance to the synapse line was computed and the average lysosomal distance was measured. This distance was normalized with the maximum distance found in the T cell. Thus, we obtained a polarity index between 1 (lysosomes at the synapse) and 0 (lysosomes at the opposite of the synapse). To measure actin/GAM enrichment at the synapse, a mask of the cortical region was defined and the mean actin intensity at the synaptic cortex was measured and compared to the mean actin intensity in the total cortex.

Mouse systemic tumour model.

We used 8- to 12-week-old NOD/SCID/IL-2Rγ- null (NSG) male mice (Jackson Laboratory), under a protocol approved by the MSKCC Institutional Animal Care and Use Committee. For the ALL models, a total of $0.5x10^6$ FFLuc-GFP NALM6/WT or NALM6/12-4 cells were administered by tail vein injection per mouse. Four days later, of $0.5x10^6$ or $0.4x10^6$ *TRAC*-HIT or *TRAC*-CAR T cells were administered by tail vein injection per mouse, respectively. For the MM model, a total of $4x10^6$ FFLuc-mCherry MM1S cells were administered by tail vein injection per mouse. Seven days later, $0.2x10^6$ *TRAC*-HIT or *TRAC*-CAR T cells were administered by tail vein injection per mouse. For the AML model, a total of $1x10^6$ FFLuc-GFP MOLM13 cells were administered by tail vein injection per mouse. Four days later, $0.4x10^6$ *TRAC*-HIT or RV-CAR T cells were administered by tail vein injection per mouse. Tumour burden was measured by bioluminescence imaging using the Xenogen IVIS Imaging System (Xenogen). Living Image software (Xenogen) was used to analyse acquired bioluminescence data. The survival end point of the mouse experiment varies depending on the tumor model (20-60 days for NALM6, 20-100 days for MOLM13, or 60-150 days for MM1S) and is determined when the

animal shows clear clinical signs of distress. Maximum tumor burden is defined by hindlimb paralysis or other clinical signs of distress, at which point the animal must be euthanized. There were no instances at which this maximum was exceeded.

Bone marrow analyses.

For the NALM6/12 mouse model, 5 mice per group were euthanized at day 10 or day 17, and bone marrow cells were isolated as described.[6] Cells were stained for CD45 (APC-Cy7), HIT or CAR (AF647), CD4 (BUV395), CD8 (PE-Cy7), PD1 (BV480), TIM3 (BV785), LAG3 (PercP-eFluor710), CD19 (BUV737) and GFP (tumour cells) and analysed by FACS in the presence of counting beads (Countbright; Invitrogen).

Statistics.

All experimental data are presented as mean ± s.e.m. No statistical methods were used to predetermine sample size. Appropriate statistical tests were used to analyze data, as described in the figure legends. Statistical analysis was performed on GraphPad Prism 7 software and R. Single-cell CTL (micro-well) assay was evaluated using test of proportions. Cytotoxicity analysis in the CTL assay was performed using two-way ANOVA or repeated measures ANOVA followed by Tukey's multiple comparison test. The cytokine level between two groups were compared using Mann-Whitney U test. Significance was set at $p < 0.05$.

Extended Data

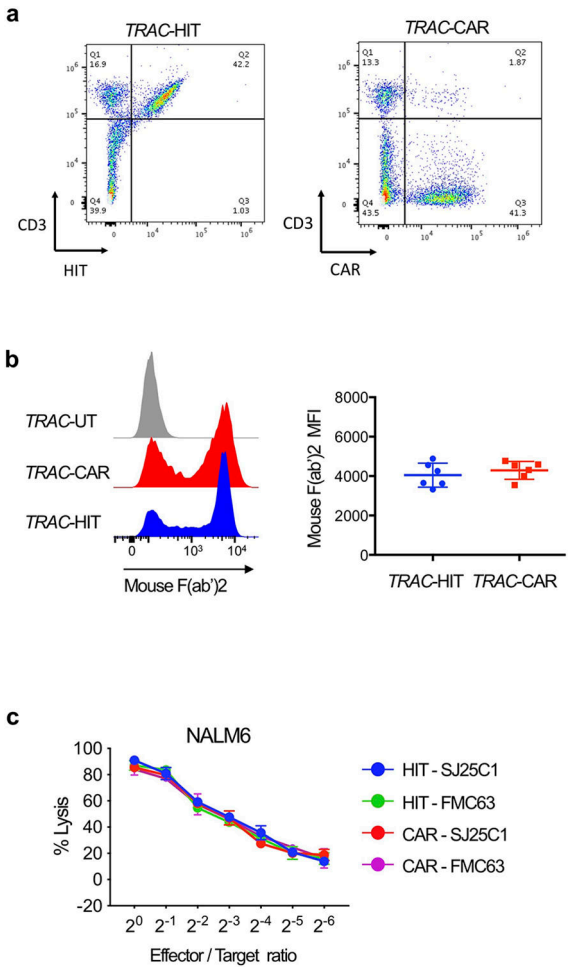

Extended Data Fig. 1. HIT receptor expression driven by the TCRα promoter rescues CD3 expression and directs lysis of CD19+ target cells.

a. Representative flow cytometry analysis showing HIT, CAR, and CD3 expression. *TRAC*-HIT and *TRAC*-CAR T cells were generated as in Fig. 1b. CD3 surface expression is only observed in *TRAC*-HIT T cells due to the presence of Cα and Cβ in the HIT receptor. **b.** HIT/CAR mean fluorescence intensity (MFI) measured by FACS using AF647-GAM. (left) HIT/CAR histograms (representative experiment) and (right) HIT/CAR MFI; n = 6 independent experiments, 3 donors. **c.** Representative cytotoxic activity using an 18 h bioluminescence assay, using firefly luciferase (FFL)-expressing NALM6 as targets cells (n = 2 independent experiments on 3 healthy donors). CD19-specific *TRAC*-HIT and *TRAC*-CAR T cells were generated using two different CD19-specific binding domains, SJ25C1 and FMC63. All data are mean ± s.e.m.

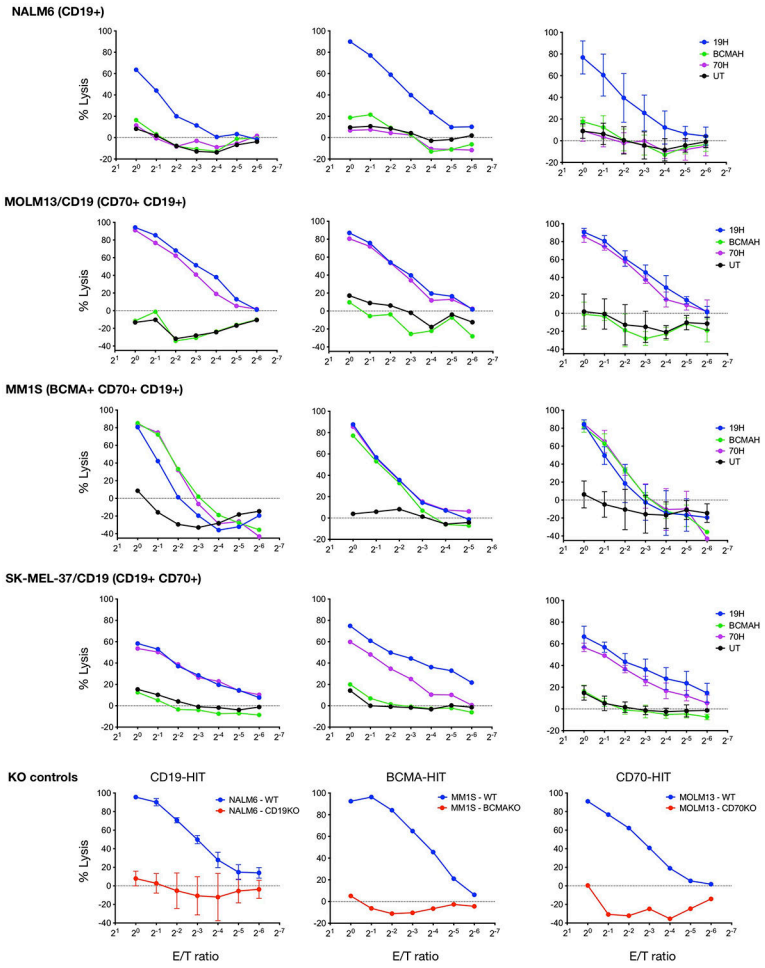

Extended Data Fig. 2. HIT receptors provide antigen-specific T cell-mediated cytotoxicity. Cytotoxic activity using an 18 h bioluminescence assay, using firefly luciferase (FFL)-expressing targets cells (n = 2 independent experiments on 2 healthy donors). CD19−, BCMA−, and CD70-specific *TRAC*-HIT T cells, and untransduced (UT) T cell controls were incubated with either NALM6 (CD19+), MOLM13/CD19 (CD70+, CD19+), MM1S (BCMA+, CD70+, CD19+), SK-MEL-37/CD19 (CD19+, CD70+), and knock-out (KO) control cell lines. CD19, BCMA, and CD70 genes were CRISPR/Cas9-edited in NALM6, MM1S, and MOLM13 cell lines, respectively. All data are mean ± s.e.m.

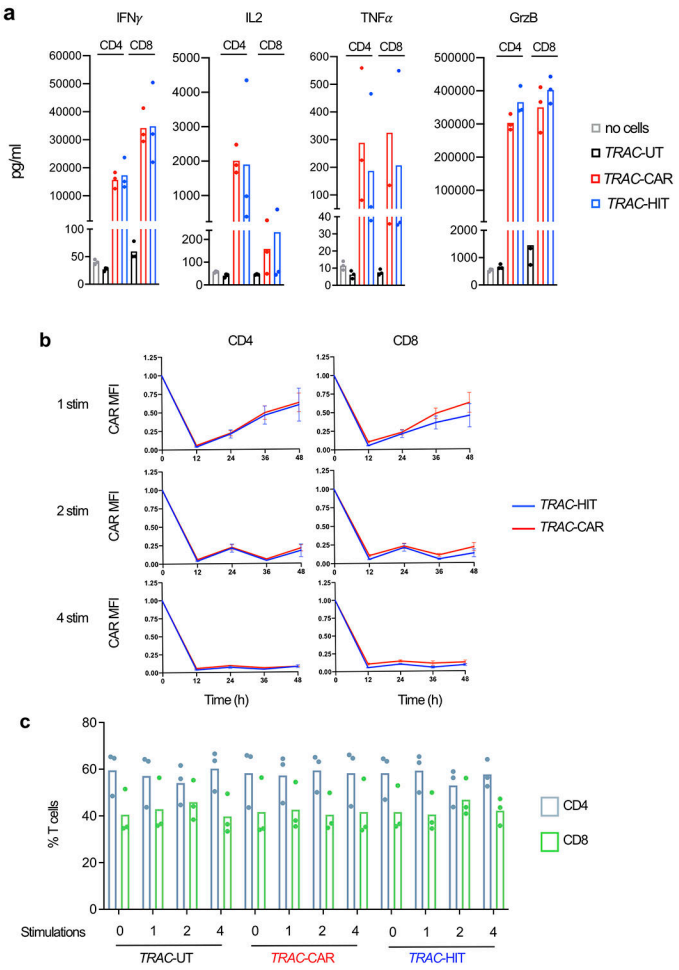

Extended Data Fig. 3. HIT receptor elicits cytokine response upon antigen stimulation; cell surface HIT receptor expression is modulated by exposure to antigen.

a. *TRAC*-Untransduced (UT), *TRAC*-HIT (HIT) and *TRAC*-CAR (CAR) T cells were stimulated on CD19+ target for 24h before supernatant were collected and analysed by flow cytometry to quantify IFNγ, IL-2, TNFα, and granzyme B (n= 3 independent experiments on 3 donors). **b.** *TRAC*-HIT and *TRAC*-CAR T cells stimulated on CD19+ target cells 1, 2 or 4 times over a 48h period were analysed by flow cytometry using the GAM, CD4, and CD8 antibodies. Plots indicate relative HIT or CAR MFI (1 = MFI at 0 h) of CD4 and CD8 *TRAC*-HIT or *TRAC*-CAR T cells, respectively. (n=3 independent experiments on 3 donors). **c.** Untransduced (UT), HIT and CAR T cells stimulated on CD19+ target cells either 0, 1, 2 or 4 times over a 48h period were analysed by flow cytometry. Plots indicate the percentage of the CAR positive T cells measured by flow cytometry analysis of CD4 and CD8 (n= 3 independent experiments on 3 donors). All data are mean ± s.e.m.

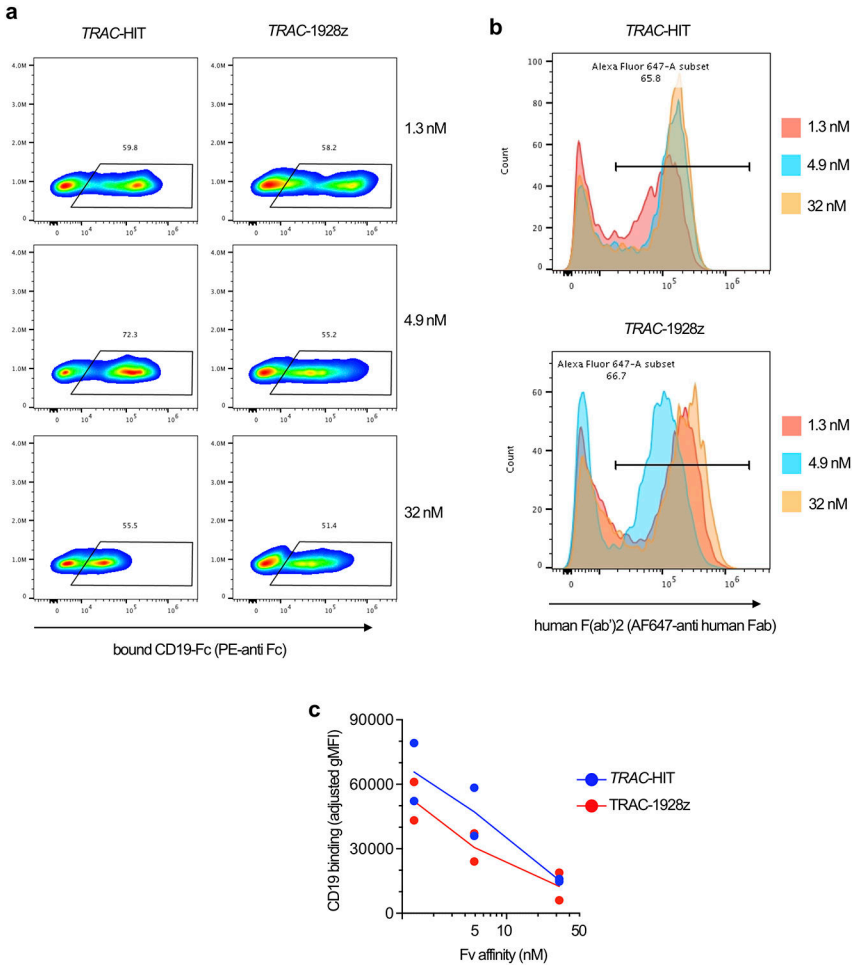

Extended Data Fig. 4. Antigen binding depends on HIT receptor affinity.

a. Representative flow cytometry analysis showing CD19 binding. *TRAC*-HIT and *TRAC*-CAR T cells were incubated with a recombinant human CD19-Fc fusion, which was then detected using an anti-hFc-PE antibody. **b.** HIT/CAR mean fluorescence intensity (MFI) measured by FACS using AF647-goat anti human (GAH) antibody (representative experiment). **c**. Plot of CD19 binding (adjusted gMFI) vs CD19 binder affinity (n=2 independent experiments). Geometric MFI for CD19 biding (PE signal from **a**.) was adjusted to the gMFI of the HIT/CAR receptor (AF647 signal from **b**.) All data are mean ± s.e.m.

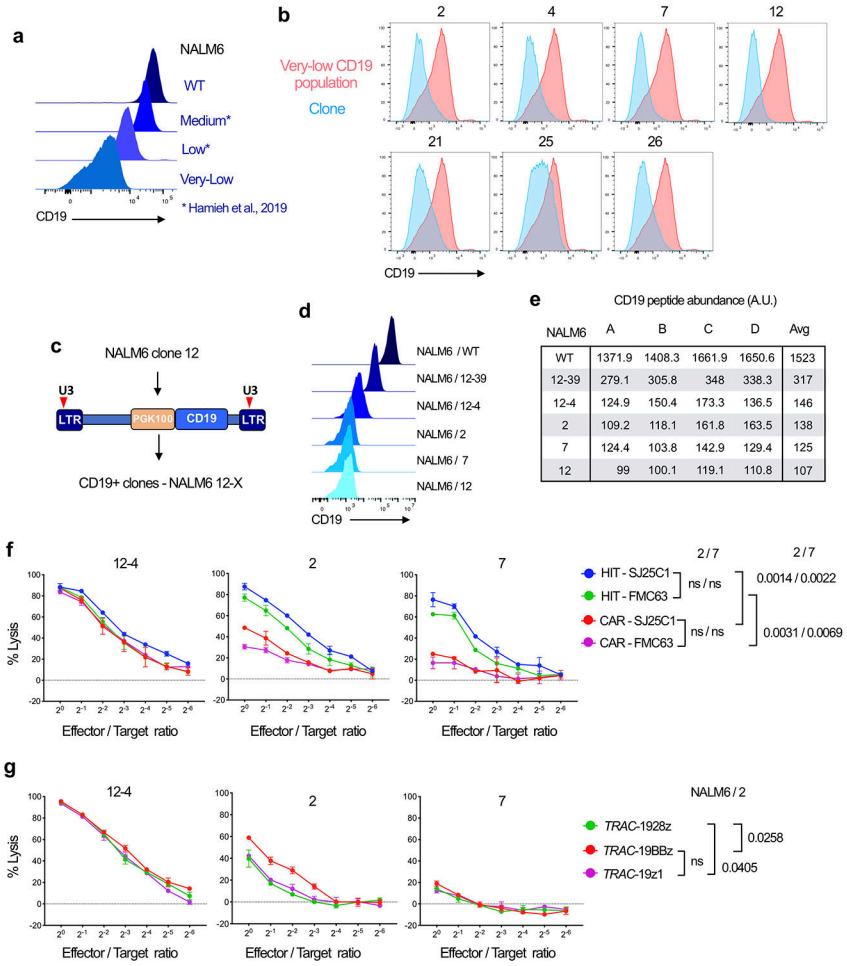

Extended Data Fig. 5. HIT receptors provide greater antigen sensitivity than CARs.

a. Representative histogram of the CD19 expression in NALM6/WT, NALM6/Medium,[21] NALM6/Low,[21] and CRISPR-edited NALM6/Very Low (this study). **b.** NALM6/Very Low cells were used to generate single cell clones by limited dilution. CD19 expression was evaluated for each clone (blue histogram) along with the initial NALM6/Very Low cell population (red histogram); clone number indicated above the histogram plot. **c.** Schematics of the SIN lentiviral vector used to express low levels of CD19 in NALM6/12 cells. PGK100: short PGK promoter, which is a weak promoter.[24] **d.** Panel of NALM6 cells expressing different CD19 levels, which is represented as a histogram. NALM6/12-4 and NALM6/12-39 are derivatives of NALM6/12, which was transduced with the lentiviral vector described in **c**. **e.** Total CD19 protein quantification using mass spectrometry. Protein levels are expressed in terms of peptide abundance (A.U.), which can be compared across all samples analysed at the same time. A-D represent 4 independent analyses. AVG, average of A-D values. **f.** Representative cytotoxic activity using an 18 h bioluminescence assay, using FFL-expressing NALM6 as targets cells (clone numbers as in **b** and **d**); n=2. CD19-specific *TRAC*-HIT and *TRAC*-CAR T cells were generated using two different CD19-specific binding domains, SJ25C1 and FMC63. Anova test was used to compare the CTL curves of all T cells for NALM6/2 and NALM6/7 cells. **g.** Representative cytotoxic activity using an

18 h bioluminescence assay, using FFL-expressing NALM6 as targets cells (same as in **f**); n=2. CD19-specific *TRAC*-1928z, *TRAC*-19BBz, and *TRAC*-19z1 T cells were prepared as described in materials and methods. Anova test was used to compare the CTL curves of all T cells for NALM6/2 cells. All data are mean ± s.e.m.

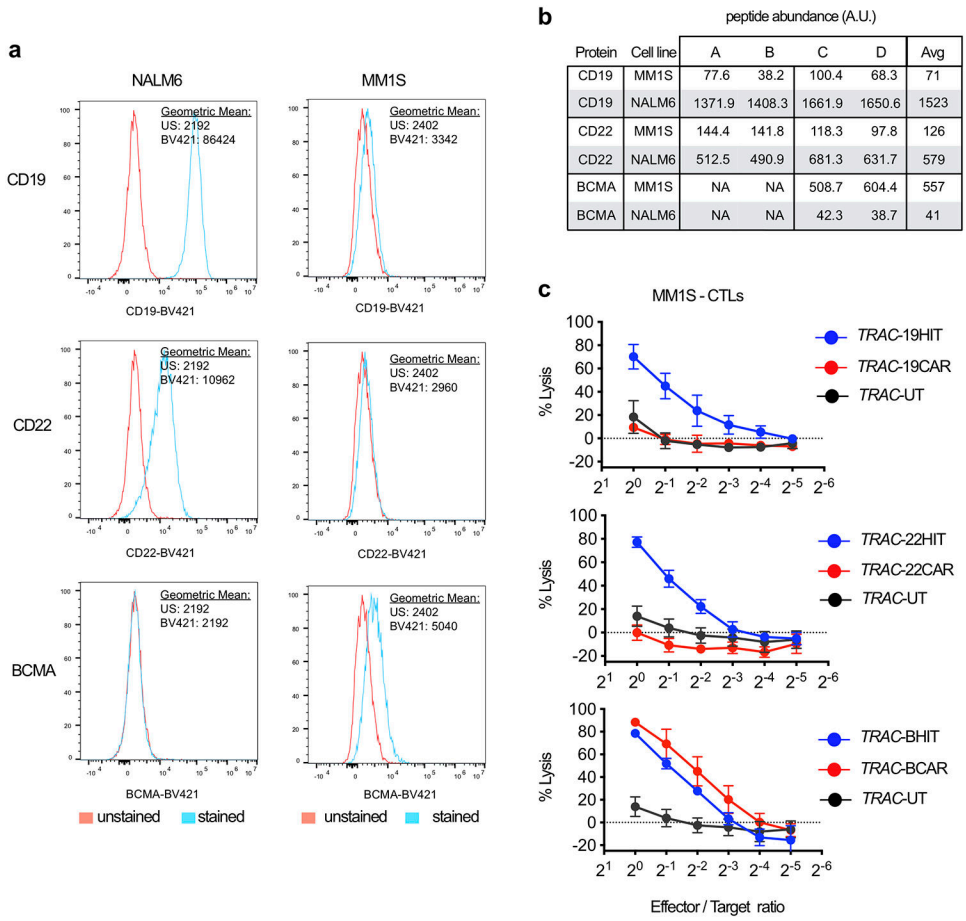

Extended Data Fig. 6. CD19, CD22, and BCMA HIT receptors elicit T cell-mediated lysis of multiple myeloma cells.

a. Representative flow cytometry analysis showing CD19, CD22, and BCMA expression in MM1S and NALM6/WT cells. **b.** Total CD19, CD22, and BCMA protein quantification using mass spectrometry. Protein levels are expressed in terms of peptide abundance (A.U.), which can be compared across all samples analysed at the same time. A-D represent 4 independent analyses. AVG, average of A-D values. **c.** Representative cytotoxic activity using an 18-h bioluminescence assay, using FFL-expressing MM1S as targets cells, which were incubated at the indicated E/T ratios with CD19−, CD22−, or BCMA-specific *TRAC*-HIT and *TRAC*-CAR T cells; n=3. All data are mean ± s.e.m. Additional specificity studies are shown in Extended Data Fig. 2.

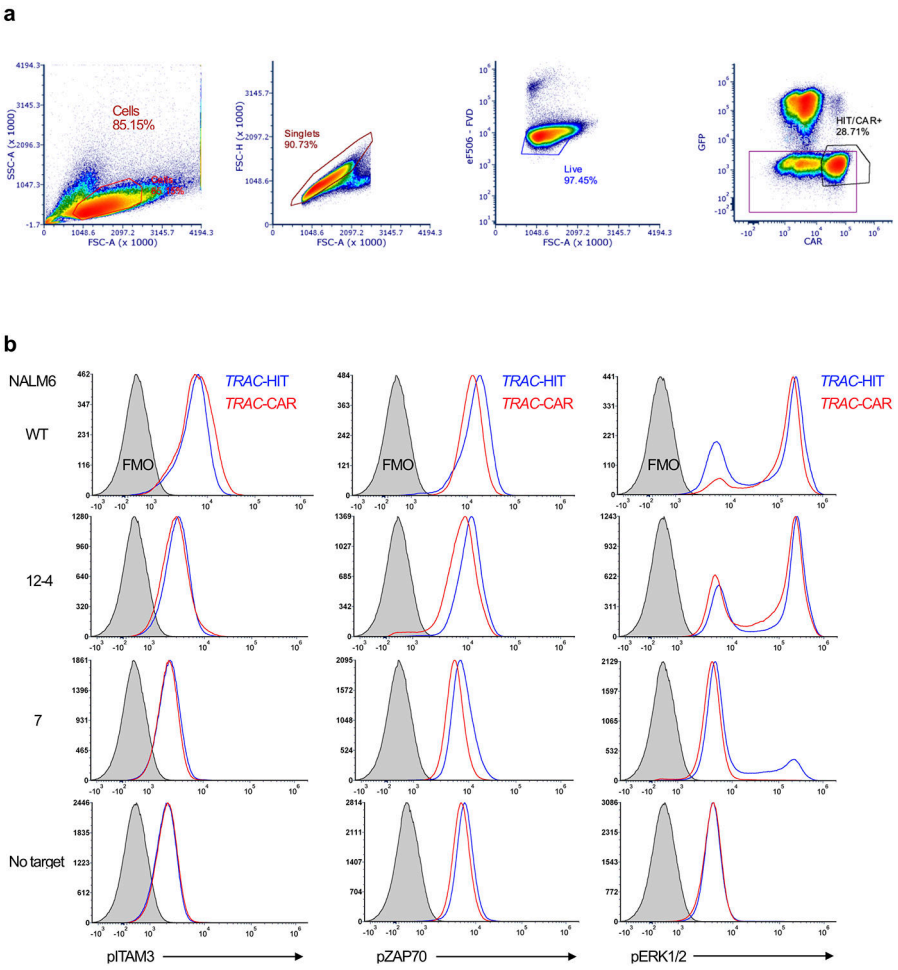

Extended Data Fig. 7. HIT T cells show increased signalling response to low antigen levels.

a. Gating strategy used to quantify ITAM3, ZAP70, and ERK1/2 phosphorylation in *TRAC*-HIT/CAR T cells (histograms shown in **b**.). **b**. Representative flow cytometry analysis showing histograms for intracellular phospho-ITAM3, phospho-ZAP70, and phospho-ERK1/2 in *TRAC*-HIT (left) and *TRAC*-CAR (right) T cells when incubated with NAML6/WT, NALM6/12-4, or NALM6/7 target cells at 1:2 ratio for 15 min, or with no target (No stim.). FMO: fluorescence minus one control. Geometric MFIs were obtained for each curve, and used to generate the plots presented in Fig 2g. All data are mean ± s.e.m.

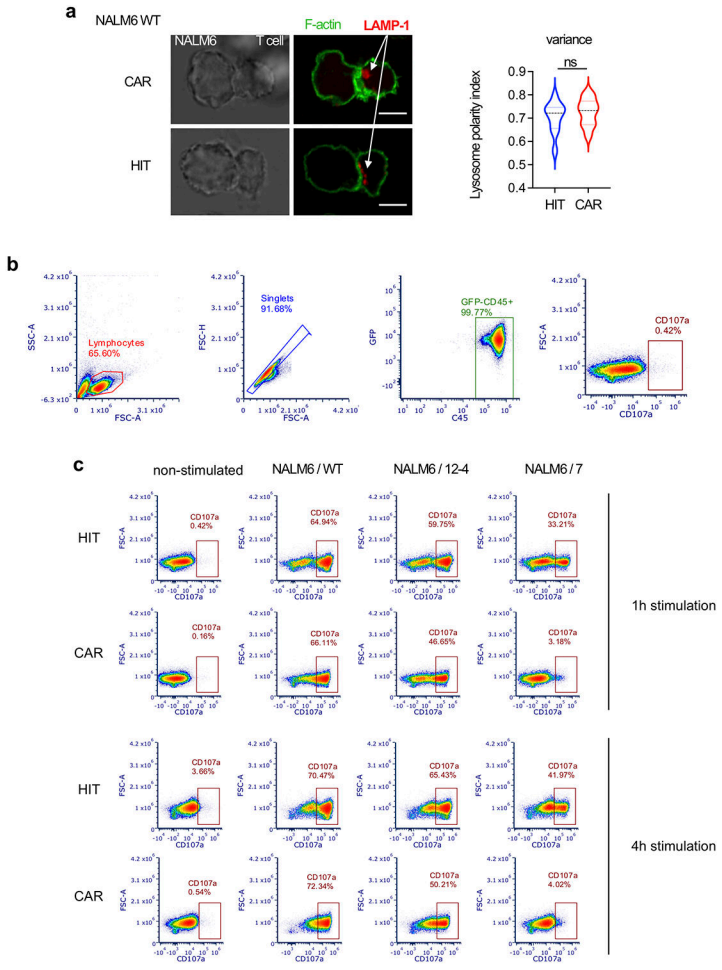

Extended Data Fig. 8. HIT T cells display increased degranulation upon stimulation.

a. Confocal and bright field images of conjugates of T cells expressing the CAR or HIT receptor and interacting for 30 min with NALM6/WT cells labeled for LAMP1 (red channel) and Alexa Fluor 546 phalloidin (actin staining showed in green). Quantification of the lysosome polarity assessed as the distance to the immune synapse and compared with the average lysosomal distance to the total cortex of the T cell. This distance was normalized with the maximum distance found in the T cell and expressed as a polarity index between 1 (lysosomes at the synapse) and 0 (lysosomes at the opposite of the synapse. Data from two independent experiments; n=59. Variance p-values were obtained by using unpaired t-test analysis. All data are mean ± s.e.m. Scale bar = 5μm. White arrows indicate LAMP-1 signal. **b.** FACS plot gates used to quantify T cell degranulation (CD107a+ cells). **b.** Representative (n=2 independent experiments) analyses of CD107a levels in *TRAC*-HIT (top) and *TRAC*-CAR (bottom) T cells when incubated for 1h (left) or 4h (right) without or with NALM6 targets of different CD19 levels.

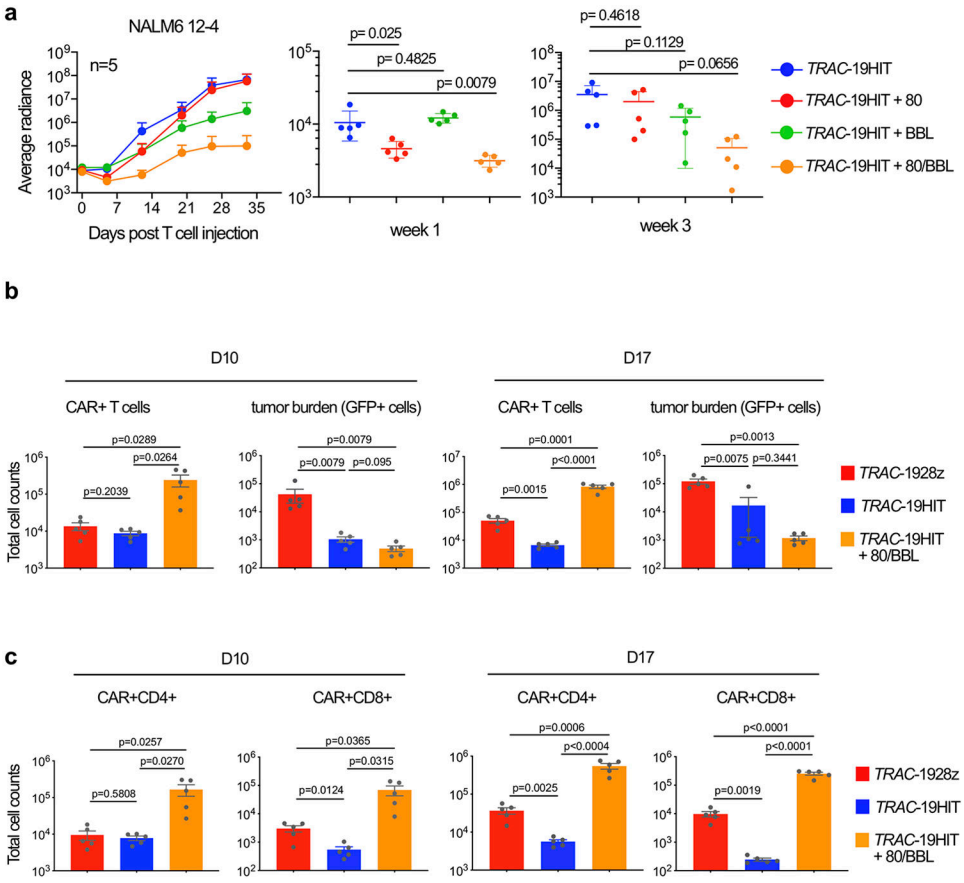

Extended Data Fig. 9. Control of low-antigen tumours by HIT T cells is enhanced by extending T cell persistence by co-expression of CD80 and 4-1BBL.

a. NALM6/12-4-bearing mice were treated with 4x10^5 *TRAC*-HIT T cells co-expressing the annotated costimulatory ligand. Tumour burden was quantified weekly over a 35-day period, at week 1 or week 3. Each line represents 5 mice. **b.** NALM6/12-4-bearing mice were treated with 4×10^5 CAR T cells (n=5 per group; dot = one mouse) and euthanized at days 10 and 17 after infusion; bone marrow *TRAC*-HIT or *TRAC*-CAR T cells and NALM6 cells were analysed and counted by FACS. **c.** Same as in **b**, except that bone marrow *TRAC*-HIT or *TRAC*-CAR CD4 and CD8 T cells counted by FACS. Two-tailed unpaired Student's *t*-tests were used for statistical analyses. All data are mean ± s.e.m. Tumor burden of individual animals are shown in Supplementary Fig. 2.

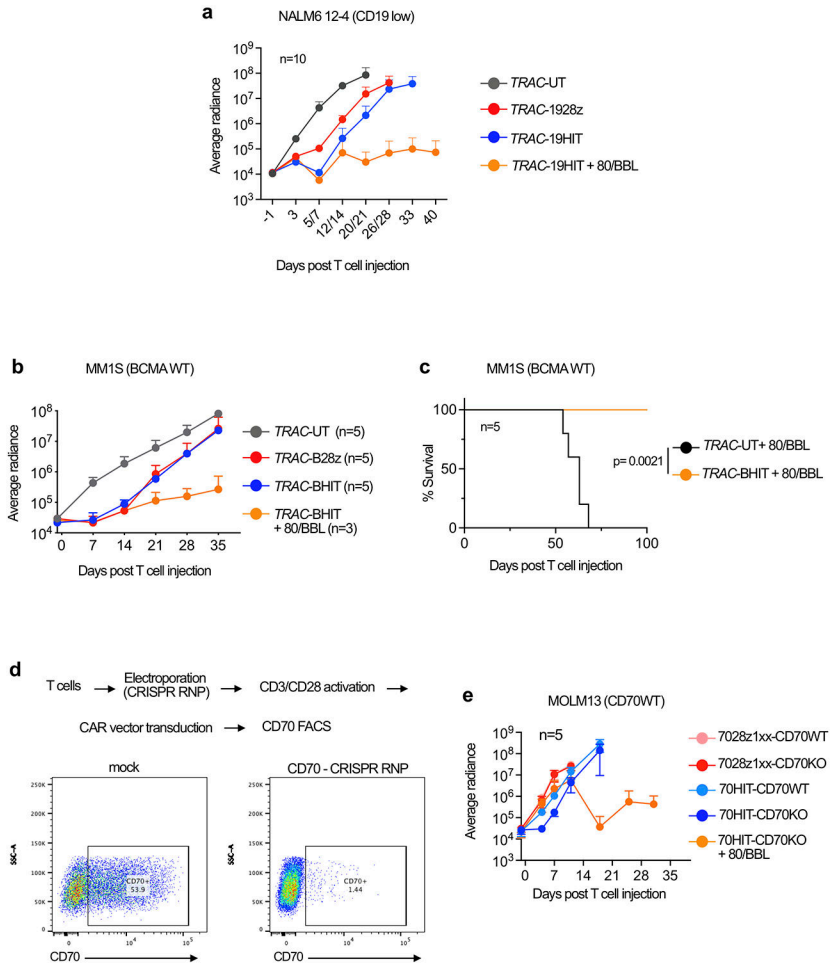

Extended Data Fig. 10. Co-expression of costimulatory ligands CD80 and 4-1BBL enhances the therapeutic potential of HIT cells.

a. Tumour burden (average radiance) of NALM6/12-4-bearing mice treated with 4×10^5 *TRAC*-HIT or *TRAC*-CAR T cells ($n = 5$), analysed through a 35-day period. **b.** Tumour burden (average radiance) of MM1S-bearing mice treated with 2×10^5 *TRAC*-HIT or *TRAC*-CAR T cells ($n = 5$), analysed through a 35-day period.

c. Kaplan-Meier analysis of survival of MM1S-bearing mice treated with 4×10^5 BCMA-specific *TRAC*-HIT or *TRAC*-HIT+80/BBL T cells ($n = 5$). **d.** Representative FACS plots of surface CD70 expression in activated CAR-T cells 4 days after electroporation without (mock) or with CD70-specific CRISPR/Cas9 RNP. **e.** Tumour burden (average radiance) of MOLM13-bearing mice treated with 4×10^5 *TRAC*-HIT or *RV*-CAR T cells ($n = 5$), analysed through a 35-day period. All data are mean ± s.e.m. Tumor burden of individual animals are shown in Supplementary Figs. 2,3.

Supplementary Material

Refer to Web version on PubMed Central for supplementary material.

Acknowledgements

We thank G. Gunset for logistical and technical assistance. We also thank the SKI Cell Therapy and Cell Engineering (CTCEF), Molecular Cytology, Flow Cytometry, Integrated Genomics Operation, Microchemistry and Proteomics, Antitumor Assessment and Animal Core Facilities for their expert assistance. This work was supported by the Lake Road Foundation, the Lymphoma and Leukemia Society, the Pasteur-Weizmann/Servier award, the Leopold Griffuel award and the NCI Cancer Center Support Grant P30 CA008748. SKI cores were in part supported by the Tow Foundation, Cycle for Survival, the Marie-Josée and Henry R. Kravis Center for Molecular Oncology and NCI grant P30 CA08748. A.D., M.S and T.G. were supported by fellowships from The Canadian Institutes of Health Research, the Fogarty Foundation and the Alexander S. Onassis Public Benefit Foundation, respectively.

Data Availability.

All requests for raw and analyzed preclinical data and materials will be promptly reviewed by the corresponding authors (M.S. and J.M.S.) to determine if they are subject to intellectual property or confidentiality obligations. Any data and materials that can be shared will be released via a material transfer agreement (requested to Michel Sadelain). Sequences for the TRAC-HIT receptors have been submitted under patent no. WO2019157454A1 (19HIT). The TRAC-HIT sequences can be found in the Supplementary Information file.

Code Availability.

We have generated scripts for the automated analyses of the single-cell CTL assays as well as the actin, CAR, HIT, and LAMP-1 signals in the confocal images. Request for these scripts will be promptly reviewed by the corresponding authors (M.S. and J.M.S.) to determine if they are subject to intellectual property or confidential obligations. Any script that can be shared will be released via a material transfer agreement (requested to Michel Sadelain).

References

1. Sadelain M, Riviere I & Riddell S Therapeutic T cell engineering. Nature 545, 423–431, doi:10.1038/nature22395 (2017). [PubMed: 28541315]
2. Eshhar Z et al. The T-body approach: potential for cancer immunotherapy. Springer seminars in immunopathology 18, 199–209, doi:10.1007/BF00820666 (1996). [PubMed: 8908700]
3. Sadelain M, Riviere I & Brentjens R Targeting tumours with genetically enhanced T lymphocytes. Nature reviews. Cancer 3, 35–45, doi:10.1038/nrc971 (2003). [PubMed: 12509765]
4. Maher J, Brentjens RJ, Gunset G, Riviere I & Sadelain M Human T-lymphocyte cytotoxicity and proliferation directed by a single chimeric TCRzeta /CD28 receptor. Nature biotechnology 20, 70–75, doi:10.1038/nbt0102-70 (2002).
5. van der Stegen SJ, Hamieh M & Sadelain M The pharmacology of second-generation chimeric antigen receptors. Nature reviews. Drug discovery 14, 499–509, doi:10.1038/nrd4597 (2015). [PubMed: 26129802]
6. June CH & Sadelain M Chimeric Antigen Receptor Therapy. The New England journal of medicine 379, 64–73, doi:10.1056/NEJMra1706169 (2018). [PubMed: 29972754]
7. Brudno JN & Kochenderfer JN Chimeric antigen receptor T-cell therapies for lymphoma. Nat Rev Clin Oncol 15, 31–46, doi:10.1038/nrclinonc.2017.128 (2018). [PubMed: 28857075]
8. Turtle CJ et al. CD19 CAR-T cells of defined CD4+:CD8+ composition in adult B cell ALL patients. J Clin Invest 126, 2123–2138, doi:10.1172/JCI85309 (2016). [PubMed: 27111235]
9. Fry TJ et al. CD22-targeted CAR T cells induce remission in B-ALL that is naive or resistant to CD19-targeted CAR immunotherapy. Nature medicine 24, 20–28, doi:10.1038/nm.4441 (2018).

10. Brudno JN et al. T Cells Genetically Modified to Express an Anti-B-Cell Maturation Antigen Chimeric Antigen Receptor Cause Remissions of Poor-Prognosis Relapsed Multiple Myeloma. Journal of clinical oncology : official journal of the American Society of Clinical Oncology 36, 2267–2280, doi:10.1200/JCO.2018.77.8084 (2018). [PubMed: 29812997]
11. Cohen AD et al. B cell maturation antigen-specific CAR T cells are clinically active in multiple myeloma. J Clin Invest 129, 2210–2221, doi:10.1172/JCI126397 (2019). [PubMed: 30896447]
12. Maude SL et al. Tisagenlecleucel in Children and Young Adults with B-Cell Lymphoblastic Leukemia. The New England journal of medicine 378, 439–448, doi:10.1056/NEJMoa1709866 (2018). [PubMed: 29385370]
13. Neelapu SS et al. Axicabtagene Ciloleucel CAR T-Cell Therapy in Refractory Large B-Cell Lymphoma. The New England journal of medicine 377, 2531–2544, doi:10.1056/NEJMoa1707447 (2017). [PubMed: 29226797]
14. Park JH et al. Long-Term Follow-up of CD19 CAR Therapy in Acute Lymphoblastic Leukemia. The New England journal of medicine 378, 449–459, doi:10.1056/NEJMoa1709919 (2018). [PubMed: 29385376]
15. Schuster SJ et al. Tisagenlecleucel in Adult Relapsed or Refractory Diffuse Large B-Cell Lymphoma. The New England journal of medicine 380, 45–56, doi:10.1056/NEJMoa1804980 (2019). [PubMed: 30501490]
16. Shah NN et al. CD4/CD8 T-Cell Selection Affects Chimeric Antigen Receptor (CAR) T-Cell Potency and Toxicity: Updated Results From a Phase I Anti-CD22 CAR T-Cell Trial. Journal of clinical oncology : official journal of the American Society of Clinical Oncology 38, 1938–1950, doi:10.1200/JCO.19.03279 (2020). [PubMed: 32286905]
17. Majzner RG & Mackall CL Tumor Antigen Escape from CAR T-cell Therapy. Cancer discovery 8, 1219–1226, doi:10.1158/2159-8290.CD-18-0442 (2018). [PubMed: 30135176]
18. Libert D et al. Serial evaluation of CD19 surface expression in pediatric B-cell malignancies following CD19-targeted therapy. Leukemia, doi:10.1038/s41375-020-0760-x (2020).
19. Shah NN & Fry TJ Mechanisms of resistance to CAR T cell therapy. Nat Rev Clin Oncol 16, 372–385, doi:10.1038/s41571-019-0184-6 (2019). [PubMed: 30837712]
20. Xu X et al. Mechanisms of Relapse After CD19 CAR T-Cell Therapy for Acute Lymphoblastic Leukemia and Its Prevention and Treatment Strategies. Front Immunol 10, 2664, doi:10.3389/fimmu.2019.02664 (2019). [PubMed: 31798590]
21. Hamieh M et al. CAR T cell trogocytosis and cooperative killing regulate tumour antigen escape. Nature 568, 112–116, doi:10.1038/s41586-019-1054-1 (2019). [PubMed: 30918399]
22. Majzner RG et al. Tuning the Antigen Density Requirement for CAR T-cell Activity. Cancer discovery 10, 702–723, doi:10.1158/2159-8290.CD-19-0945 (2020). [PubMed: 32193224]
23. Priceman SJ et al. Co-stimulatory signaling determines tumor antigen sensitivity and persistence of CAR T cells targeting PSCA+ metastatic prostate cancer. Oncoimmunology 7, e1380764, doi:10.1080/2162402X.2017.1380764 (2018). [PubMed: 29308300]
24. Eyquem J et al. Targeting a CAR to the TRAC locus with CRISPR/Cas9 enhances tumour rejection. Nature 543, 113–117, doi:10.1038/nature21405 (2017). [PubMed: 28225754]
25. Feucht J et al. Calibration of CAR activation potential directs alternative T cell fates and therapeutic potency. Nature medicine 25, 82–88, doi:10.1038/s41591-018-0290-5 (2019).
26. Zhao Z et al. Structural Design of Engineered Costimulation Determines Tumor Rejection Kinetics and Persistence of CAR T Cells. Cancer cell 28, 415–428, doi:10.1016/j.ccell.2015.09.004 (2015). [PubMed: 26461090]
27. Lee DW et al. T cells expressing CD19 chimeric antigen receptors for acute lymphoblastic leukaemia in children and young adults: a phase 1 dose-escalation trial. Lancet 385, 517–528, doi:10.1016/S0140-6736(14)61403-3 (2015). [PubMed: 25319501]
28. Purbhoo MA, Irvine DJ, Huppa JB & Davis MM T cell killing does not require the formation of a stable mature immunological synapse. Nature immunology 5, 524–530, doi:10.1038/ni1058 (2004). [PubMed: 15048111]
29. Sykulev Y, Joo M, Vturina I, Tsomides TJ & Eisen HN Evidence that a single peptide-MHC complex on a target cell can elicit a cytolytic T cell response. Immunity 4, 565–571, doi:10.1016/s1074-7613(00)80483-5 (1996). [PubMed: 8673703]

30. Brentjens RJ et al. Eradication of systemic B-cell tumors by genetically targeted human T lymphocytes co-stimulated by CD80 and interleukin-15. Nature medicine 9, 279–286, doi:10.1038/nm827 (2003).
31. Maude SL et al. Chimeric antigen receptor T cells for sustained remissions in leukemia. The New England journal of medicine 371, 1507–1517, doi:10.1056/NEJMoa1407222 (2014). [PubMed: 25317870]
32. Gross G, Waks T & Eshhar Z Expression of immunoglobulin-T-cell receptor chimeric molecules as functional receptors with antibody-type specificity. Proceedings of the National Academy of Sciences of the United States of America 86, 10024–10028, doi:10.1073/pnas.86.24.10024 (1989). [PubMed: 2513569]
33. Kuwana Y et al. Expression of chimeric receptor composed of immunoglobulin-derived V regions and T-cell receptor-derived C regions. Biochem Biophys Res Commun 149, 960–968, doi:10.1016/0006-291x(87)90502-x (1987). [PubMed: 3122749]
34. Sher BT, Nairn R, Coligan JE & Hood LE DNA sequence of the mouse H-2Dd transplantation antigen gene. Proceedings of the National Academy of Sciences of the United States of America 82, 1175–1179, doi:10.1073/pnas.82.4.1175 (1985). [PubMed: 3856254]
35. Baeuerle PA et al. Synthetic TRuC receptors engaging the complete T cell receptor for potent anti-tumor response. Nat Commun 10, 2087, doi:10.1038/s41467-019-10097-0 (2019). [PubMed: 31064990]
36. Helsen CW et al. The chimeric TAC receptor co-opts the T cell receptor yielding robust anti-tumor activity without toxicity. Nat Commun 9, 3049, doi:10.1038/s41467-018-05395-y (2018). [PubMed: 30076299]
37. Xu Y et al. A novel antibody-TCR (AbTCR) platform combines Fab-based antigen recognition with gamma/delta-TCR signaling to facilitate T-cell cytotoxicity with low cytokine release. Cell Discov 4, 62, doi:10.1038/s41421-018-0066-6 (2018). [PubMed: 30479831]
38. Liu Y et al. Chimeric STAR receptors using TCR machinery mediate robust responses against solid tumors. Sci Transl Med 13, doi:10.1126/scitranslmed.abb5191 (2021).
39. MacKay M et al. The therapeutic landscape for cells engineered with chimeric antigen receptors. Nature biotechnology 38, 233–244, doi:10.1038/s41587-019-0329-2 (2020).
40. Gaud G, Lesourne R & Love PE Regulatory mechanisms in T cell receptor signalling. Nat Rev Immunol 18, 485–497, doi:10.1038/s41577-018-0020-8 (2018). [PubMed: 29789755]
41. Matza D et al. A scaffold protein, AHNAK1, is required for calcium signaling during T cell activation. Immunity 28, 64–74, doi:10.1016/j.immuni.2007.11.020 (2008). [PubMed: 18191595]
42. Schwartzberg PL, Mueller KL, Qi H & Cannons JL SLAM receptors and SAP influence lymphocyte interactions, development and function. Nat Rev Immunol 9, 39–46, doi:10.1038/nri2456 (2009). [PubMed: 19079134]
43. Randzavola LO et al. Loss of ARPC1B impairs cytotoxic T lymphocyte maintenance and cytolytic activity. J Clin Invest 129, 5600–5614, doi:10.1172/JCI129388 (2019). [PubMed: 31710310]
44. Stephan MT et al. T cell-encoded CD80 and 4-1BBL induce auto- and transcostimulation, resulting in potent tumor rejection. Nature medicine 13, 1440–1449, doi:10.1038/nm1676 (2007).
45. Nguyen P et al. Route of 41BB/41BBL Costimulation Determines Effector Function of B7-H3-CAR.CD28ζ T Cells. Molecular Therapy - Oncolytics 18, 202–214, doi:10.1016/j.omto.2020.06.018 (2020). [PubMed: 32728609]
46. Perna F et al. Integrating Proteomics and Transcriptomics for Systematic Combinatorial Chimeric Antigen Receptor Therapy of AML. Cancer cell 32, 506–519 e505, doi:10.1016/j.ccell.2017.09.004 (2017). [PubMed: 29017060]
47. Riether C et al. Targeting CD70 with cusatuzumab eliminates acute myeloid leukemia stem cells in patients treated with hypomethylating agents. Nature medicine 26, 1459–1467, doi:10.1038/s41591-020-0910-8 (2020).
48. Brugnoni D et al. CD70 expression on T-cell subpopulations: study of normal individuals and patients with chronic immune activation. Immunol Lett 55, 99–104, doi:10.1016/s0165-2478(96)02693-4 (1997). [PubMed: 9143940]

49. Kimachi K, Croft M & Grey HM The minimal number of antigen-major histocompatibility complex class II complexes required for activation of naive and primed T cells. European journal of immunology 27, 3310–3317, doi:10.1002/eji.1830271230 (1997). [PubMed: 9464819]

50. Henrickson SE et al. T cell sensing of antigen dose governs interactive behavior with dendritic cells and sets a threshold for T cell activation. Nature immunology 9, 282–291, doi:10.1038/ni1559 (2008). [PubMed: 18204450]

51. Dong R et al. Rewired signaling network in T cells expressing the chimeric antigen receptor (CAR). EMBO J 39, e104730, doi:10.15252/embj.2020104730 (2020). [PubMed: 32643825]

52. Liu X et al. A Chimeric Switch-Receptor Targeting PD1 Augments the Efficacy of Second-Generation CAR T Cells in Advanced Solid Tumors. Cancer Res 76, 1578–1590, doi:10.1158/0008-5472.CAN-15-2524 (2016). [PubMed: 26979791]

53. Oda SK et al. A CD200R-CD28 fusion protein appropriates an inhibitory signal to enhance T-cell function and therapy of murine leukemia. Blood 130, 2410–2419, doi:10.1182/blood-2017-04-777052 (2017). [PubMed: 29042364]

Methods-Only References

54. Hendel A et al. Chemically modified guide RNAs enhance CRISPR-Cas genome editing in human primary cells. Nature biotechnology 33, 985–989, doi:10.1038/nbt.3290 (2015).

55. Papapetrou EP et al. Genomic safe harbors permit high beta-globin transgene expression in thalassemia induced pluripotent stem cells. Nature biotechnology 29, 73–78, doi:10.1038/nbt.1717 (2011).

56. Rivière I, Brose K & Mulligan RC Effects of retroviral vector design on expression of human adenosine deaminase in murine bone marrow transplant recipients engrafted with genetically modified cells. Proc. Natl Acad. Sci. USA 92, 6733–6737 (1995). [PubMed: 7624312]

57. Navarrete-Perea J, Yu Q, Gygi SP & Paulo JA Streamlined Tandem Mass Tag (SL-TMT) Protocol: An Efficient Strategy for Quantitative (Phospho)proteome Profiling Using Tandem Mass Tag-Synchronous Precursor Selection-MS3. Journal of proteome research 17, 2226–2236, doi:10.1021/acs.jproteome.8b00217 (2018). [PubMed: 29734811]

58. Zucchetti AE, Bataille L, Carpier JM, Dogniaux S, San Roman-Jouve M, Maurin M, Stuck MW, Rios RM, Baldari CT, Pazour GJ, Hivroz C Tethering of vesicles to the Golgi by GMAP210 controls LAT delivery to the immune synapse. Nat Commun. 10, 2864. doi:10.1038/s41467-019-10891-w (2019). [PubMed: 31253807]

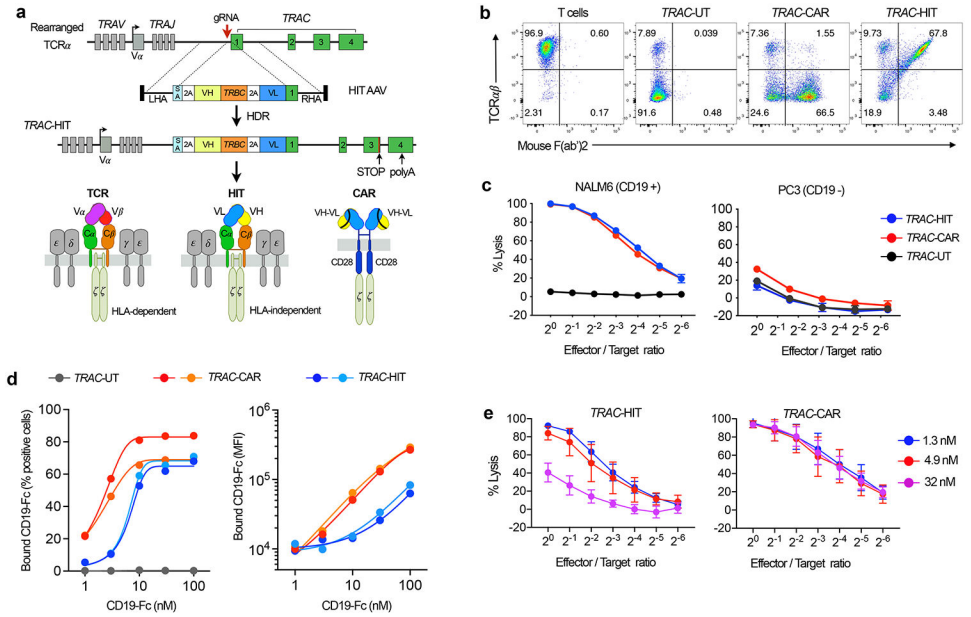

Figure 1. *TRAC* locus editing to create an HLA-independent TCR (HIT receptor) directs TCR/CD3 complex-mediated antigen recognition

a. Schematic of the targeting strategy to generate a HIT receptor in situ at the *TRAC* locus. The targeting construct (HIT-AAV) contains a splice acceptor, followed by P2A cleaving peptide and the CD19-specifc HIT gene elements (a V_H-Cβ gene followed by P2A and the V_L gene), which are joined to the *TRAC* exon 1; all flanked by sequences homologous to the *TRAC* locus (left and right homology arm: LHA and RHA). Once integrated, the V_H-Cβ and V_L-Cα expression is driven by the endogenous TCRα promoter and polyA elements, while TCRα expression is disrupted. V_H-Cβ and V_L-Cα chains will associate to form the HIT heterodimer. The TCR/CD3 complex is depicted to highlight the similarities and contrast between HIT and TCR. The 19-28z CAR, utilizing the same V_H and V_L elements in the format of an scFv, is also depicted. TRAV: TCR alpha variable region. TRAJ: TCR alpha joining region. SA: Splice acceptor. P2A: *Porcine teschovirus* 2A sequence. **b.** Representative TCRαβ/F(ab')2 flow plot 4 days after transfection of T cells with *TRAC*-targeting CRISPR/Cas9 and HIT or CAR AAV6 transduction. **c.** Cytotoxic activity using an 18-hr bioluminescence assay. Firefly luciferase (FFL)- and CD19-expressing NALM6 (left), or FFL-expressing PC3 (CD19 negative, right) as targets cells (n=2 biological independent samples); additional specificity studies are shown in Extended Data Fig 2. **d**. Binding capacity of HIT and CAR T cells measured by titrating CD19-Fc fusion. *TRAC*-HIT and *TRAC*-CAR T cells from 2 different donors were incubated with a recombinant human CD19-Fc fusion, which was then detected using an anti-hFc-PE antibody. Left panel: % positive cells detected; right panel: mean fluorescent intensity (MFI) of the bound CD19-Fc. **e**. Representative cytotoxic activity using an 18 h bioluminescence assay, using firefly luciferase (FFL)-expressing NALM6 as targets cells (n = 4 independent experiments on 4 healthy donors). CD19-specific *TRAC*-HIT and *TRAC*-CAR T cells were generated using three different binding domains specific to a CD19 epitope but of distinct affinities (1.3, 4.9, and 32 nM). All data are mean ± s.e.m.

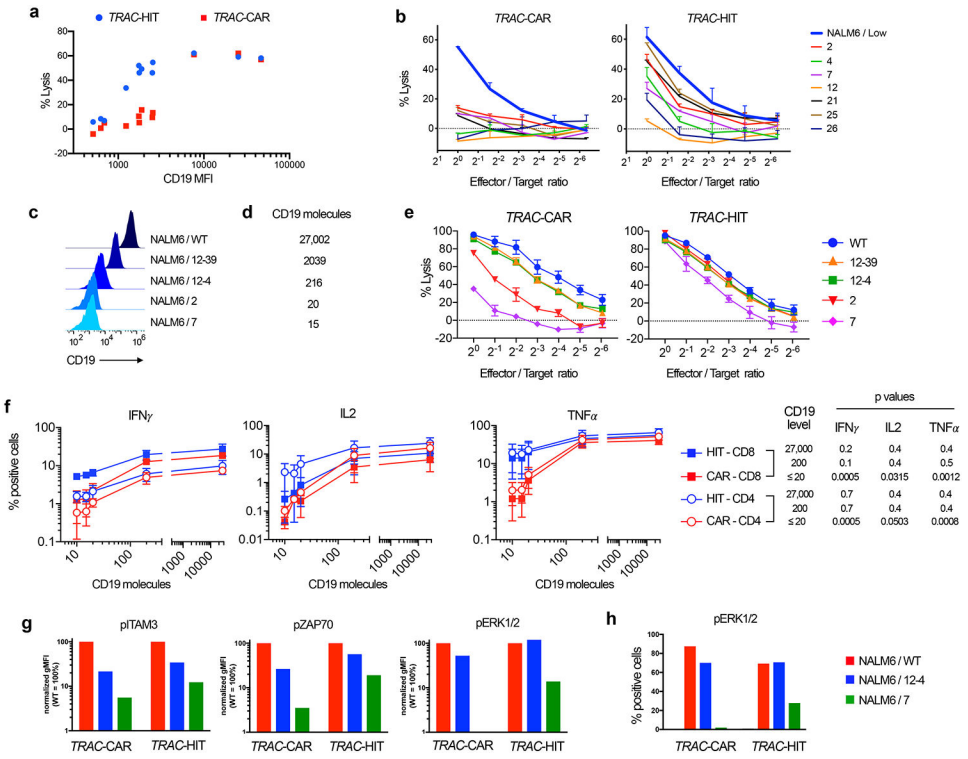

Figure 2. *TRAC*-HIT T cells exhibit increased sensitivity for tumour cells expressing low antigen levels relative to *TRAC*-CAR T cells.

a. Cytotoxic activity using a 4-hr bioluminescence assay at a 1:1 ratio of *TRAC*-HIT/ *TRAC*-CAR T cells (effectors) and FFL+NALM6 cells expressing different CD19 surface levels (targets). (Average killing and MFI from $n = 2$ independent experiments on 2 donors). **b.** Representative cytotoxic activity using an 18 h bioluminescence assay, using FFL-expressing NALM6 clones as targets cells (clone numbers as in Extended Data Fig. 5b); NALM6/Low was used as positive control; n=2 biological independent samples. **c.** CD19 flow histograms for WT and NALM6 clones expressing decreasing levels of CD19. **d.** Quantification of surface CD19 levels using FACS and PE-calibration beads. NALM6 cells were stained PE-anti CD19 antibody. CD19 geometric MFIs (gMFIs) for NALM6/WT, NALM6/12-39, and NALM6/12-4 were used to determine the number of CD19 molecules per cells using the standard curve obtained with the calibration beads. CD19 gMFIs for NALM6/2, NALM6/7, NALM6/12 were used to establish a ratio with NALM6/12-4 since their values were outside the linear range of the standard curve. **e.** Cytotoxic activity using an 18-h bioluminescence assay at different effector:target ratios for *TRAC*-HIT/*TRAC*-CAR T cells and FFL+NALM6 cells expressing different CD19 surface levels (panel **c**); n=2 biological independent samples. **f.** Percentage of *TRAC*-HIT or *TRAC*-CAR T cells (both CD4 and CD8 cells) with positive expression of IFNγ, IL-2 or TNFα after intracellular staining after co-culture with NALM6 clones expressing the indicated levels of CD19. Right, Mann-Whitney p values when using NALM6 WT (27,000), NALM6 12-4 (200), and NALM6 12, 7, and 2 (≤20) target cells. n= 3 independent experiments on 3 different T cell donors. **g.** and **h.** Levels of phospho-ITAM3, phospho-ZAP70, or phospho-ERK1/2 in *TRAC*-HIT or *TRAC*-CAR T cells when incubated with NALM6 WT, 12-4 or 7

targets at a 1:2 ratio. **g.** Levels are presented as a percentage of the signal detected in T cells incubated with NALM6 WT target. **h.** Percentage of *TRAC*-HIT or *TRAC*-CAR T cells containing phospho-ERK1/2. **g.** and **h.** The data presented are representative of 2 independent experiments using 2 different T cell healthy donors. Except for **g.** and **h.** all data are mean ± s.e.m.

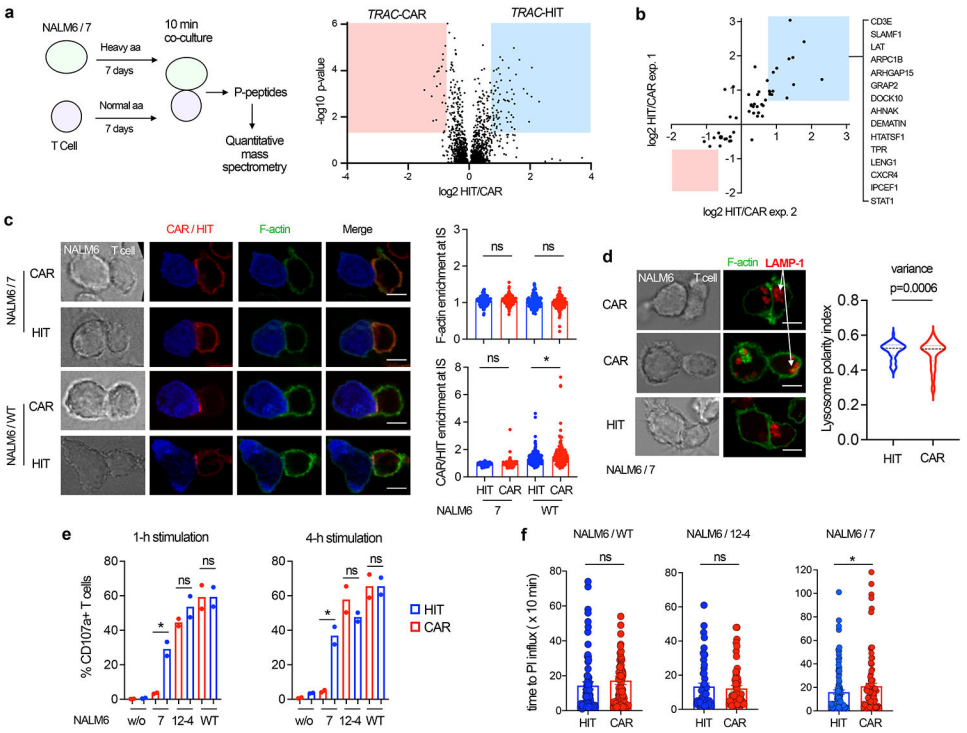

Figure 3. *TRAC*-HIT T cells exhibit increased degranulation and rapid killing activity upon exposure to low antigen levels.

a. Summary of the quantitative phospho-proteomic analysis. Heavy amino acid-labelled NALM6/7 cells were incubated with either *TRAC*-HIT or *TRAC*-CAR T cells for 10 min. Purified phospho (P)-peptides were analysed by mass spectrometry. Volcano plot shows total and enriched P-peptides in *TRAC*-HIT (blue square) and *TRAC*-CAR (red square) T cells. **b.** P-peptides (two independent experiments; two different healthy T cell donors) with a $p<0.05$ ($-\log10>1.3$) are plotted as log2 HIT/CAR (experiment 1 vs experiment 2); p-values were calculated by paired t-test analysis (integrated in Proteome Discoverer software). P-peptides enriched in *TRAC*-HIT (blue square) T cells are shown at the right. **c**. Representative confocal and bright field images of conjugates of CAR or HIT T cells interacting for 30 min with NALM6/7 or NALM6/WT cells (blue) labeled with goat anti-mouse (red) and phalloidin (green). Quantification of actin (upper panel) and CAR/HIT (lower panel) mean fluorescence intensity at the immune synapse region, divided by the mean intensity measured in the total T cell cortex. Each dot represents one cell; horizontal lines=median. Scale bars=5μm. Data from two independent experiments; n=60. **P<0.01, ns: non-significant (Mann-Withney test). **d.** Confocal and bright field images of CAR or HIT T cell conjugates interacting for 30 min with NALM6/7 cells labeled for LAMP1 (red) and actin (green). Quantification of lysosome polarity (distance to the immune synapse compared to average lysosomal distance to the total T cell cortex). This distance was normalized with the maximum distance found in the T cell and expressed as a polarity index between 1 (lysosomes at the synapse) and 0 (lysosomes at the opposite of the synapse). Data from two independent experiments; n=59. P-values obtained by unpaired t-test analysis. Scale bars=5μm. White arrows indicate LAMP-1 signal. **e.** Degranulation measured by CD107a staining upon incubating HIT/CAR T cells for 1h and 4h with NALM6 cells

of different CD19 levels. P-values obtained by unpaired t-test analysis; n=2 biological independent samples, and data is representative of 2 independent experiments. Asterisk (*) represents a p value of <0.05. **f.** Single-cell time-lapse imaging cytotoxicity assay. Time from conjugate formation to propidium iodide (PI) influx in target cells; left: NALM6/WT (HIT, n=93; CAR, n=78), middle NALM6/12-4 (HIT, n=53; CAR, n=57), right NALM6/7 (HIT, n=104; CAR, n=94). For each target cell: 2 independent experiments with 2 T cell donors. P-values obtained by unpaired t-test analysis; asterisk (*) means p<0.05; ns: not significant. All data are mean ± s.e.m.

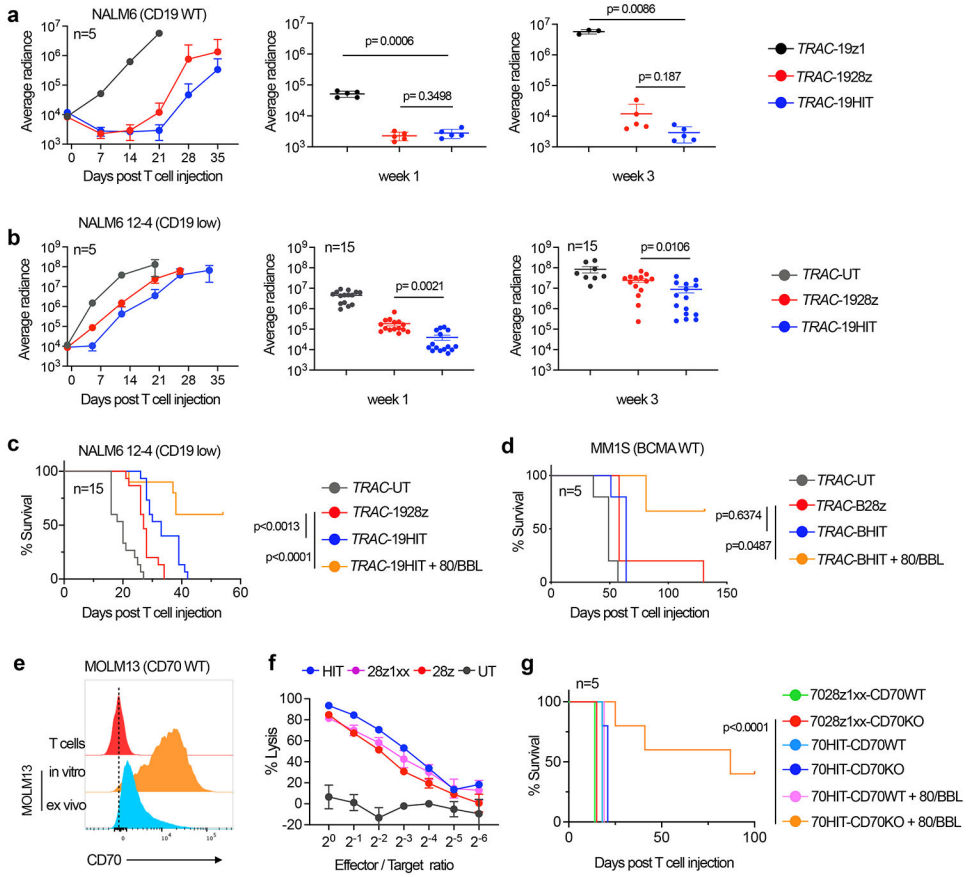

Figure 4. *TRAC*-HIT T cells outperform *TRAC*-CAR T cells in controlling low-antigen tumour cells *in vivo*.

a. Tumour burden (average radiance) of NALM6 WT-bearing mice treated with 5×10^5 *TRAC*-HIT or *TRAC*-CAR T cells ($n = 5$), analysed through a 35-day period, at week 1 or week 3. Quantification is the average photon count of ventral and dorsal acquisitions per animal at all given time points. A two-tailed unpaired t-test was used to compare each group pair. **b.** Tumour burden (average radiance) of NALM6/12-4-bearing treated with 4×10^5 *TRAC*-HIT or *TRAC*-CAR T cells ($n = 15$), analysed through a 35-day period, at week 1 or week 3. A two-tailed unpaired t-test was used to compare each group pair. **c.** Kaplan-Meier analysis of survival of NALM6/12-4-bearing mice treated with 4×10^5 *TRAC*-HIT or *TRAC*-CAR T cells ($n = 15$). **d.** Kaplan-Meier analysis of survival of MM1S-bearing mice treated with 2×10^5 *TRAC*-HIT or *TRAC*-CAR T cells ($n = 5$). **e.** CD70 flow histograms for MOLM13 cells *in vitro* and *ex-vivo* (from mouse bone marrow samples), and non-activated T cells (negative control). **f**. Cytotoxic activity using an 18-h bioluminescence assay at different effector:target ratios for *TRAC*-70HIT/*RV*-CAR T cells (7028z and 7028z1xx) and FFL+ MOLM13 cells; n=3. Additional specificity studies are shown in Extended Data Fig. 2. **g.** Kaplan-Meier analysis of survival of MOLM13-bearing mice treated with 4×10^5 *TRAC*-HIT or *TRAC*-CAR T cells ($n = 5$). **c, d, and g.** *P* values were determined by a log-rank Mantel-Cox test (survival). All data are mean ± s.e.m. Tumor burden of individual animals are shown in Supplementary Figs. 1-3.